



MINISTÉRIO DA CIÊNCIA, TECNOLOGIA, INOVAÇÕES E COMUNICAÇÕES
INSTITUTO NACIONAL DE PESQUISAS ESPACIAIS

sid.inpe.br/mtc-m21b/2017/02.02.16.01-TDI

THE ROLE OF POPULATION II AND III STARS IN THE COSMIC CHEMICAL EVOLUTION

Lia Camargo Corazza

Master's Dissertation of the Graduate Course in Astrophysics, guided by Drs. Oswaldo Duarte Miranda, and Carlos Alexandre Wuensche de Souza, approved in February 21, 2017.

URL of the original document:

<<http://urlib.net/8JMKD3MGP3W34P/3NAADHH>>

INPE
São José dos Campos
2017

PUBLISHED BY:

Instituto Nacional de Pesquisas Espaciais - INPE

Gabinete do Diretor (GB)

Serviço de Informação e Documentação (SID)

Caixa Postal 515 - CEP 12.245-970

São José dos Campos - SP - Brasil

Tel.:(012) 3208-6923/6921

Fax: (012) 3208-6919

E-mail: pubtc@inpe.br

**COMMISSION OF BOARD OF PUBLISHING AND PRESERVATION
OF INPE INTELLECTUAL PRODUCTION (DE/DIR-544):**

Chairperson:

Maria do Carmo de Andrade Nono - Conselho de Pós-Graduação (CPG)

Members:

Dr. Plínio Carlos Alvalá - Centro de Ciência do Sistema Terrestre (CST)

Dr. André de Castro Milone - Coordenação de Ciências Espaciais e Atmosféricas (CEA)

Dra. Carina de Barros Melo - Coordenação de Laboratórios Associados (CTE)

Dr. Evandro Marconi Rocco - Coordenação de Engenharia e Tecnologia Espacial (ETE)

Dr. Hermann Johann Heinrich Kux - Coordenação de Observação da Terra (OBT)

Dr. Marley Cavalcante de Lima Moscati - Centro de Previsão de Tempo e Estudos Climáticos (CPT)

Silvia Castro Marcelino - Serviço de Informação e Documentação (SID) **DIGITAL**

LIBRARY:

Dr. Gerald Jean Francis Banon

Clayton Martins Pereira - Serviço de Informação e Documentação (SID)

DOCUMENT REVIEW:

Simone Angélica Del Ducca Barbedo - Serviço de Informação e Documentação (SID)

Yolanda Ribeiro da Silva Souza - Serviço de Informação e Documentação (SID)

ELECTRONIC EDITING:

Marcelo de Castro Pazos - Serviço de Informação e Documentação (SID)

André Luis Dias Fernandes - Serviço de Informação e Documentação (SID)



MINISTÉRIO DA CIÊNCIA, TECNOLOGIA, INOVAÇÕES E COMUNICAÇÕES
INSTITUTO NACIONAL DE PESQUISAS ESPACIAIS

sid.inpe.br/mtc-m21b/2017/02.02.16.01-TDI

THE ROLE OF POPULATION II AND III STARS IN THE COSMIC CHEMICAL EVOLUTION

Lia Camargo Corazza

Master's Dissertation of the Graduate Course in Astrophysics, guided by Drs. Oswaldo Duarte Miranda, and Carlos Alexandre Wuensche de Souza, approved in February 21, 2017.

URL of the original document:

<<http://urlib.net/8JMKD3MGP3W34P/3NAADHH>>

INPE
São José dos Campos
2017

Cataloging in Publication Data

- Corazza, Lia Camargo.
- C81r The role of population II and III stars in the cosmic chemical evolution / Lia Camargo Corazza. – São José dos Campos : INPE, 2017.
xvi + 83 p. ; (sid.inpe.br/mtc-m21b/2017/02.02.16.01-TDI)
- Dissertation (Master in Astrophysics) – Instituto Nacional de Pesquisas Espaciais, São José dos Campos, 2017.
- Guiding : Drs. Oswaldo Duarte Miranda, and Carlos Alexandre Wuensche de Souza.

1. Cosmic chemical evolution. 2. Structure formation.
3. Population III. 4. Population II. 5. Cosmology. I.Title.

CDU 52-36



Esta obra foi licenciada sob uma Licença [Creative Commons Atribuição-NãoComercial 3.0 Não Adaptada](https://creativecommons.org/licenses/by-nc/3.0/).

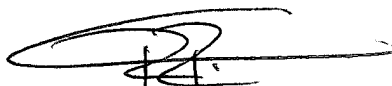
This work is licensed under a [Creative Commons Attribution-NonCommercial 3.0 Unported License](https://creativecommons.org/licenses/by-nc/3.0/).

Aluno (a): **Lia Camargo Corazza**

Título: "THE ROLE OF POPULATION II AND III STARS IN THE COSMIC CHEMICAL EVOLUTION"

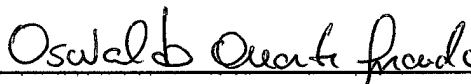
Aprovado (a) pela Banca Examinadora
em cumprimento ao requisito exigido para
obtenção do Título de **Mestre** em
Astrofísica

Dr. Reinaldo Ramos de Carvalho



Presidente / INPE / SJC Campos - SP

Dr. Oswaldo Duarte Miranda



Orientador(a) / INPE / SJC Campos - SP

Dr. Carlos Alexandre Wuensche de Souza



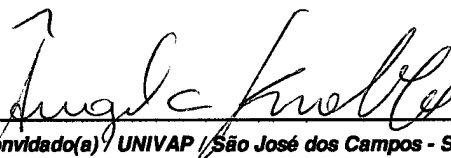
Orientador(a) / INPE / SJC Campos - SP

Dr. Roberto Dell'Aglio Dias da Costa



Convidado(a) / IAG/USP / São Paulo - SP

Dra. Angela Cristina Krabbe



Convidado(a) / UNIVAP / São José dos Campos - SP

Este trabalho foi aprovado por:

() maioria simples

unanimidade

São José dos Campos, 21 de fevereiro de 2017

*“To see a world in a grain of sand
And a heaven in a wild flower,
Hold infinity in the palm of your hand
And eternity in an hour”.*

WILLIAM BLAKE
in “*Auguries of Innocence*”, 1863

AGRADECIMENTOS

Ao meu orientador, Dr. Oswaldo Miranda, por toda a atenção dedicada ao projeto, pelas reuniões, discussões, pelo constante incentivo e por sua admirável dedicação com seus alunos e com a pesquisa.

Ao meu co-orientador, Dr. Carlos Alexandre Wuensche, por todos os momentos de discussão e ideias para o projeto, pela dedicação e incentivo.

Aos meus pais, Alexandre e Mirna, agradeço com todo o meu coração pelo apoio, amor, carinho, incentivo e suporte em todas as minhas escolhas e às minhas irmãs, Carol e Camila, pelo companheirismo, amor e carinho.

Aos meus amigos, primeiramente Dudu e Rafael, companheiros de turma que tive a sorte de conhecer e dividir todos os momentos de aprendizado, amadurecimento e também de diversão ao longo dos dois últimos anos. Agradeço também aos amigos que ajudaram diretamente no desenvolvimento do trabalho, principalmente à Carol, Nina, David e à todos os amigos da pós-graduação. Ao Marcelo, meu agradecimento com muito carinho por todo os momentos de companheirismo, incentivo e apoio.

Aos Professores e Pesquisadores da DAS que, sempre muito disponíveis, fizeram parte essencial de todo o aprendizado adquirido e do trabalho desenvolvido nos dois últimos anos.

Aos funcionários do INPE, sempre muito solícitos fazendo com que nosso dia-a-dia seja mais prazeroso dentro da Instituição.

À CAPES, pelo apoio financeiro.

ABSTRACT

In this work we present a semi-analytical Chemical Evolution Model in the Cosmological Framework for 11 elements, taking into account the evolution of Population III and II stars and the transition between metallicities $Z = 0$ and $10^{-6}, 10^{-4}, 10^{-3}, 4.10^{-3}, 8.10^{-3}$ and $2.10^{-2}Z_{\odot}$. We calculate the star formation rate in the framework of hierarchical structure formation (PEREIRA; MIRANDA, 2010) coupled with chemical evolution equations for Oxygen (O), Iron (Fe), Zinc (Zn), Nickel (Ni), Silicon (Si), Magnesium (Mg), Aluminum (Al), Carbon (C), Nitrogen (N), Phosphorus (P) and Sulphur (S). The best results are reached when considering a Press-Schechter-like formalism, a Salpeter IMF ($x = 1.35$) and $\tau_s = 2Gyr$ as time-scale for star formation (VITTI, 2012). We compare data generated by the model with chemical abundances in the gas-phase from Damped Lyman- α Systems (DLAs). Zn is underabundant probably due to the lack of Hypernovae (HNe) yields in the code, while P and Ni are underabundant probably because Supernovae type Ia (SNe Ia) yields are not taken into account. Al and Mg are discussed to be underabundant because of chemical abundances measurement problems in DLAs (such as blending with the Ly- α Forest) while Fe and Si are thought to be overabundant because of dust depletion effects on these systems. C , N and O are unexpectedly overabundant and although C and O are used as fuel in SNe Ia, this mechanism is probably not enough to remove significant amount of these elements from the Inter-galactic Medium (IGM), leaving the possibility for further studies on the influence of Carbon-enhanced Metal-Poor stars (CEMPs), Carbon planets formation in the early Universe and the appearance of life on the Chemical Cosmic Evolution (LOEB, 2016).

Palavras-chave: Cosmic Chemical Evolution. Structure Formation. Population III. Population II. Cosmology.

O PAPEL DAS ESTRELAS DE POPULAÇÃO III E II NA EVOLUÇÃO QUÍMICA CÓSMICA

RESUMO

Neste trabalho apresentamos um modelo semi-analítico de Evolução Química no Contexto Cosmológico para 11 elementos, considerando a evolução das estrelas de População III e II e a transição entre as metalicidades $Z = 0, 10^{-6}, 10^{-4}, 10^{-3}, 4.10^{-3}, 8.10^{-3}$ e $2.10^{-2}Z_{\odot}$. Calculamos a taxa de formação estelar no cenário hierárquico de formação de estruturas (PEREIRA; MIRANDA, 2010) acoplado à equações de evolução química para o Oxigênio (O), Ferro (Fe), Zinco (Zn), Níquel (Ni), Silício (Si), Magnésio (Mg), Alumínio (Al), Carbono (C), Nitrogênio (N), Fósforo (P) e Enxofre (S). Os melhores resultados são atingidos considerando-se um formalismo do tipo Press-Schechter, uma função de massa inicial (IMF) do tipo Salpeter e $\tau_s = 2Gyr$ para a escala de tempo da formação estelar (VITTI, 2012). Comparamos os dados gerados pelo modelo com abundâncias químicas na fase do gás de *Damped Lyman- α Systems* (DLAs). Resultados mostram subabundância para o Zn provavelmente pela falta de yields de Hypenovae no código, enquanto P e Ni estão subabundantes provavelmente pelo fato de que yields de Supernovar tipo Ia (SNe Ia) não são considerados. Devido à problemas em medidas de DLAs, (como por exemplo “blendind” com as linhas da Floresta Ly- α), Al e Mg estão subabundantes enquanto Fe e Si estão sobreabundantes provavelmente devido à influência de depleção por poeira na determinação das abundâncias nos dados observacionais nos DLAs. C , N and O aparecem inesperadamente sobreabundantes, e embora C e O sejam usados como combustível em SNe Ia, esse mecanismo provavelmente não é suficiente para retirar quantidades significativas destes elementos do Meio Inter-galático (IGM), abrindo a possibilidade para futuros estudos sobre a influência das *Carbon-enhanced Metal-Poor stars* (CEMPs), planetas de Carbono no Universo Primordial e do aparecimento de vida na Evolução Química Cósmica (LOEB, 2016).

Palavras-chave: Evolução Química Cósmica. Formação de Estruturas. População III. População II. Cosmologia.

LIST OF FIGURES

	<u>Page</u>
2.1 Millenium Simulation for Cosmic Structure Formation (Virgo Consortium/Springel et al. (2005)).	5
2.2 Code	23
3.1 Remnants in the Heger e Woosley (2002) for Pop III stars.	32
3.2 Schematic view of the transition between Populations (National Science Foundation and NASA)	36
3.3 The Lyman- α Forest (not redshift corrected) http://www.hs.uni-hamburg.de/jliske/qsoal/	38
3.4 Metal line transitions in the DLA towards B0105-008. From Ellison et al. (2012)	39
4.1 Yields for Pop III Stars according to the progenitor mass.	42
4.2 Decisions of the code for the Transition between Populations	44
4.3 Chemical Evolution for Zinc	49
4.4 Chemical Evolution for Zinc - detail	50
4.5 Yields from Pop III for 500 and 1000 M_{\odot} stars (OHKUBO et al., 2006)	51
4.6 Yields for Pop III original mass branches compared to Ohkubo et al. (2006) yields for 500 and 1000 M_{\odot} stars.	51
4.7 Chemical Evolution for Aluminum	52
4.8 Chemical Evolution for Aluminum - detail	53
4.9 Chemical Evolution for Magnesium	55
4.10 Chemical Evolution for Magnesium - detail	55
4.11 Chemical Evolution for Phosphorus	56
4.12 Chemical Evolution for Phosphorus - detail	57
4.13 Chemical Evolution for Nickel	57
4.14 Chemical Evolution for Nickel - detail	58
4.15 Chemical Evolution for Iron	59
4.16 Chemical Evolution for Iron - detail	60
4.17 Chemical Evolution for Silicon	60
4.18 Chemical Evolution for Silicon - detail	61
4.19 Depletion of Iron on DLAs	62
4.20 Depletion of Iron on DLAs - Detail	62
4.21 Chemical Evolution for Oxygen	63
4.22 Chemical Evolution for Nitrogen	64
4.23 Chemical Evolution for Carbon	64

4.24 Chemical Evolution for Sulphur	66
4.25 Chemical Evolution for Sulphur - detail	66
4.26 Total Metallicity	68
4.27 Total Metallicity	69
4.28 Total Metallicity	69

LIST OF TABLES

	<u>Page</u>
4.1 Element abundances in the present-day solar photosphere from Asplund (2009)	45
4.2 Redshifts at which the model reaches the Metallicities used in the code for the Transition of Populations.	67
5.1 Possibilities of abundances problems in the code.	72

CONTENTS

	<u>Page</u>
1 INTRODUCTION	1
2 THE FORMATION OF STRUCTURES	3
2.1 Comoving coordinates	5
2.2 Density Perturbations	6
2.2.1 Newtonian Approximation	7
2.2.2 Perturbation Analysis	8
2.3 Solutions	11
2.4 Formation of Dark Matter Halos	12
2.4.1 Virialized Halos	15
2.5 Press-Schechter Formalism	17
2.6 The Initial Mass Function (IMF) and the Star Formation Rate (SFR)	20
3 ASPECTS RELATED TO THE CHEMICAL ENRICHMENT OF THE UNIVERSE	25
3.1 Stellar Evolution and Nucleosynthesis	25
3.1.1 The Evolution of Single Stars	26
3.1.2 Nucleosynthesis Chains	27
3.1.3 Remnants	31
3.1.4 Stellar Yields	32
3.2 Chemical Evolution Models	33
3.3 Transition from Population III to Population II Stars	34
3.3.1 Population III Stars	34
3.3.2 Transition and Critical Metallicity	35
3.4 Damped Lyman- α Systems - Observational Data	37
3.4.1 Properties of Damped Lyman- α Systems	37
3.4.2 Depletion	39
4 METHODOLOGY AND RESULTS	41
4.1 Methodology	41
4.2 Using Damped Lyman- α Systems Chemical Abundances	44
4.3 Results and Data Discussion	48
4.3.1 The Underabundance of Zinc and Hypernovae Nucleosynthesis	49

4.3.2	The Underabundance of Aluminum	52
4.3.3	Magnesium: Underbundance or DLA Problems?	54
4.3.4	The underabundance of Phosphorus and Nickel	56
4.3.5	The Iron and Silicon Superabundance	59
4.3.6	The Carbon, Nitrogen and Oxygen Superabundances	63
4.3.7	The Sulfur Cosmic Chemical Evolution	66
4.3.8	Transition and Z_{cr}	67
5	CONCLUSIONS AND PERSPECTIVES	71
5.1	Conclusions	71
5.2	Perspectives	73
	REFERENCES	75

1 INTRODUCTION

In the beginning of the Universe, gas was predominantly constituted of the lightest elements, Hydrogen and Helium. It is estimated that only a few seconds after the Big Bang (BB) ($\sim 1000s$) until 20 minutes after it happened, the primordial nucleosynthesis formed the nuclei D (2H), 3He , 4He and a small fraction of 7Li . Due to the rapid expansion and cooling of the Universe, it was not possible to produce any other heavier element during the primordial nucleosynthesis and conditions for heavier elements to form only appeared later when the first stars began to form, around 380Myr (WMAP and Planck) after the BB. These stars started to form from that pristine gas, and due to the low cooling properties of Hydrogen and Helium, they had very high masses, quickly triggering nuclear processes in their cores and producing heavy elements, from Helium to Iron. They exceeded their cores' fuel quickly, ending their lives in powerful Supernovae explosions providing all the ingredients for the Chemical Enrichment of the Universe to take place.

Pristine gas was quickly enriched by heavy elements, increasing the metallicity of the Intergalactic Medium (IGM) and providing properties for the second generation of stars to appear. The second generation of stars kept on enriching the medium even more and the process kept on happening, giving birth to stars each generation more metal rich.

The Universe today is constituted by a huge number of galaxies and stars that are constantly evolving, thereby changing the characteristics around them. Stars host the only ideal environment for nuclear reactions to happen, transforming lighter elements into heavier ones and ejecting them into the interstellar medium when they died.

This set of stars, galaxies, galaxy clusters together form the large scale structures in the Universe. These structures were originated in the beginning of the Universe, right after the Big Bang, through perturbations in the dark matter density that grew due to gravitational instability until the first stars started to form.

Regarding the Chemical Evolution processes, models have been developed by [Tinsley e Larson \(1978\)](#), [Matteucci \(2016a\)](#) to characterize the evolution of production of metals inside the Galaxy. Our approach in this work is to couple the Galactic Chemical Evolution models into the Cosmological Framework, projecting them into the hierarchical scenario of large structure formation. We explore the theory of primordial perturbations along with the details of the Initial Mass Function and the Star Formation Rate, essential ingredients for our model. We built a semi-analytical model powerful for studying the evolution of the Total Metallicity of Universe and 11 different metals (C, N, O, Al, Si, S, Fe, Ni, Zn, P and Mg) regarding all the

processes that produce and inject them to the IGM. We choose to work with Population III, the first stars to form in the Universe only from primordial metal-free gas, and Pop II stars, the second generation of stars formed through the metallicity increasing cycles of the Universe, each generation more metal rich and with evolving nucleosynthetic properties.

The first part of the work consists in understanding how dark matter halos are formed and in calculating the Cosmic Star Formation Rate to identify what part of the available gas in the Universe become stars. It is calculated with a code written by [Pereira e Miranda \(2010\)](#) and the results give the basis to insert the chemical evolution equations, explained in [3.2](#).

Last, we explain how we compare our model with observational data for chemical abundances in Damped Lyman-alpha Systems, explore our results, the most important mechanisms for adjusting the model and the possibility of finding a Transition between Population III and II stars in the Chemical Evolution of the Universe.

2 THE FORMATION OF STRUCTURES

The Cosmological Principle states that matter in the Universe is homogeneously distributed, but we know that in fact this is only true for scales $\gtrsim 300$ Mpc. In these scales, we can say that the Universe is “unperturbed”. Observations made in smaller scales indicate that the Universe clearly presents inhomogeneities (such as galaxies, clusters, stellar systems, etc.). But what is the mechanism needed to form these structures?

In the beginning, the Universe was almost completely smooth, but tiny density deviations appeared. They are almost widely accepted as being generated by the amplification of quantum fluctuations which took place during the inflationary epoch and began to grow until reaching macroscopic proportions. The Cosmic Background Radiation, produced when the Universe was about 380.000 years old, give us information that the Universe was smooth in about one part in 10^5 :

$$\frac{\delta\rho}{\rho} \approx 10^{-5} \tag{2.1}$$

The inhomogeneities appeared soon after the Big Bang and are probably the reason we have big structures in the Universe today. The growth of such structures only happened due to gravitational instabilities. When inflation occurred, they grew and started to attract dark matter and form the first halos that later started to attract baryonic matter and form stars, galaxies, etc. Figure 2.1, for example, shows how the distribution of matter in the Universe has evolved along time according to data from the Millenium Simulation (SPRINGEL *et al.*, 2005).

The Structure Formation Theory can be divided in two classes:

- The generation of the primordial inhomogeneities, that we can call “seeds of galaxies” (and everything else we see today). This is a very complicated part of the theory. Once we are not able to observe phenomena from back then, it is a little speculative in some points. On the other hand, this part relies on inflation, a very good candidate for the origins of perturbations. The inflationary predictions agree with present observations and can continue to be tested. In the inflationary theory, quantum fluctuations in the inflaton field originated the structures.
- The study of the growth of the small homogeneities until the present structures that we observe. This part relies much more on observations and

we have a well established theory, the general relativity theory. The uncertainty in this part is in the fact that we do not know very well dark energy and dark matter, and they are the dominant part of the Universe's density and the growth of structures depend on the equation of state of these density components ¹.

This second part of the Theory can also be divided in three categories:

- **Linear Cosmological Growth**
Described by cosmic fluxes on scales bigger than 30 Mpc and associated to a density contrast (δ) smaller than 1. In this case it is possible to study the processes involved with gravitational instability and the structures of the Universe through the Linear Perturbation Theory.
- **Quasi-linear Cosmological Growth**
When a region reaches $\delta \geq 1$. In this scenario the perturbation evolution cannot be described by Linear Theory, because it involves scales from 3 to 30 Mpc.
- **Non-linear Cosmological Growth**
In this case, $\delta \gg 1$ and the scales are studied through computational simulations, where they are smaller than 3 Mpc.

Our goal at this point is to study the formation of large scale structures in the Universe through the gravitational instability that acts on small perturbations. The calculations associated with structure formation involves the determination of the density contrast $\delta_k(t_o)$ on the Fourier Space and the power spectrum $P(k)$, given by:

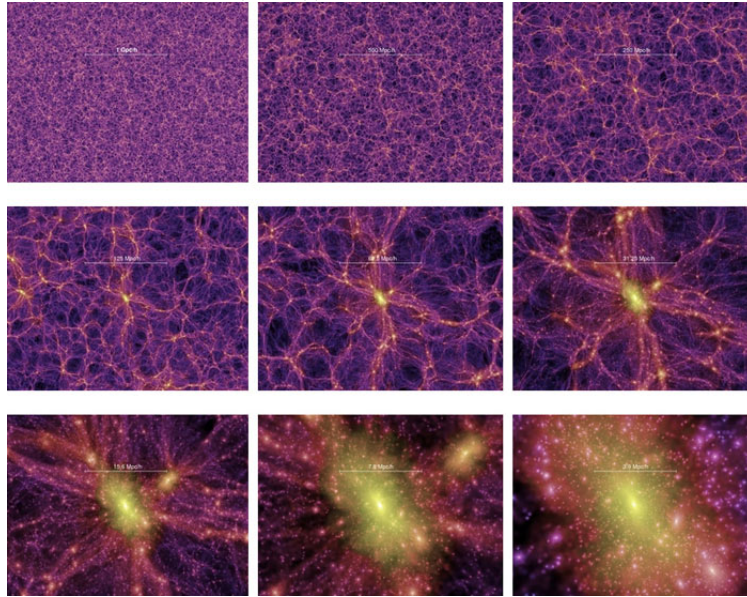
$$\delta_k(t_o) = T(k) \cdot \delta_k(t_i) \tag{2.2}$$

$$P(k) = T^2(k) \cdot P_i(k) \tag{2.3}$$

Where $P_i(k)$ is the initial power spectrum, determined from the theory responsible for the production of the perturbations (in this case, inflation) (BARDEEN et al.,

¹Dark Energy will begin to dominate the dynamics of the Universe only very close to the present epoch. On the other hand, Dark Matter starts dominating the dynamics of the Universe right after equipartition.

Figure 2.1 - Millenium Simulation for Cosmic Structure Formation (Virgo Consortium/Springel et al. (2005)).



1986) and $T(k)$ is the transfer function, which describes how the shape of the initial power spectrum is modified by different physical processes.

We now know that in order to understand the formation of structures we must understand density perturbations. On that purpose, we will analyze how an inhomogeneity can grow due to gravitational instabilities and use the Newtonian approximation described in 2.2.1. We will then be ready to understand the physics of how structures in the Universe grow. First we will talk about how the expanding Universe affects our coordinate system in 2.1. (For further details in the structure formation background see, e.g., Peebles (1993), Dodelson (2003), Padmanabhan (1993)).

2.1 Comoving coordinates

In order to discuss the evolution of the perturbations in a expanding Friedmann Robertson Walker (FRW) Universe we must consider comoving coordinates. In an expanding Universe, the expansion is governed by the Hubble expansion, being the Hubble parameter defined as follows:

$$H(t) = \frac{\dot{a}}{a} \tag{2.4}$$

Where “a” is the scale factor and on overdot denotes a time derivative, i.e.:

$$\dot{a} = \frac{da}{dt} \quad (2.5)$$

The Hubble expansion is uniform, so our space coordinate can be written as:

$$\mathbf{r} = a(t)\mathbf{x} \quad (2.6)$$

Where “r” represents the physical coordinates and “x” are the comoving coordinates. The expansion factor is such that $a(t_o) = a_o = 1$ for today and $a(t = 0) = 0$ at the time the Big Bang happened.

The comoving position is then given by:

$$\mathbf{x}(t) = \frac{\mathbf{r}(t)}{a(t)} \quad (2.7)$$

Also, a region in the Universe has a peculiar velocity that comes from the variation of $\mathbf{x}(t)$:

$$\mathbf{u} = \dot{a}(t)\mathbf{x} + \mathbf{v}, \quad \mathbf{v} \equiv a\dot{\mathbf{x}}, \quad (2.8)$$

Note that $\dot{a}(t)x$ is the Hubble flow while \mathbf{v} is the peculiar velocity which describes the fluid movement in relation to the observer. We are replacing (\vec{r}, t) for (\vec{x}, t) , then:

$$\vec{\nabla}_{\mathbf{r}} \rightarrow \frac{1}{a}\vec{\nabla}_{\mathbf{x}}; \quad \frac{\partial}{\partial t} \rightarrow \frac{\partial}{\partial t} - \frac{\dot{a}}{a}\vec{x} \cdot \vec{\nabla}_{\mathbf{x}} \quad (2.9)$$

2.2 Density Perturbations

We know that somewhere in the past there were very small inhomogeneities in our Universe that started to grow because of gravitational instabilities. While these perturbations are small, we can consider them in the linear regime. As they grow and become bigger, they have to be treated as non-linear. In this work we will be treating the first-order perturbation theory, or linear perturbation theory.

The linear regime is defined by density and velocity perturbations of a very small amplitude. This means that:

$$\delta \ll 1 \tag{2.10}$$

The density fluctuation $\delta(x, t)$ is given in terms of non-perturbed density $\bar{\rho}$ or ρ_u that is uniform and does not depend on x :

$$\delta(x, t) = \frac{\rho(x, t) - \rho_u(t)}{\rho_u(t)} \tag{2.11}$$

The formation of structures in the Universe is connected with the growth of δ in an expanding Universe. The total energy (density) $\rho(x, t)$ is the sum of various components:

$$\rho(x, t) = \rho_m(x, t) + \rho_r(x, t) + \rho_{DE}(x, t) \tag{2.12}$$

Where the subindex m is for matter (baryonic and dark components), r denoted radiation and DE stands for dark energy.

The perturbation in the Universe is then represented as:

$$\rho_u \cdot \delta(x, t) = \rho_{mu}(t) \cdot \delta_m(x, t) + \rho_{ru}(t) \cdot \delta_r(x, t) + \rho_{DE,u}(t) \cdot \delta_{DE}(x, t) \tag{2.13}$$

But for cosmological constant as the dark energy component we have:

$$\delta_{DE}(x, t) = 0 \tag{2.14}$$

In particular, the growth of structures in a scale smaller than the Hubble size can be described through the Newtonian Theory of Gravity.

2.2.1 Newtonian Approximation

The Newtonian scenario is a good approximation of general relativity in scales inside the Hubble radius and when considering non-relativistic matter. In this case,

we will use the newtonian approximation to study sub-Hubble fluctuations in the cold dark matter (CDM) and baryons after decoupling.

The equations of motion of the fluid are:

Continuity Equation:

The continuity equation (or mass conservation equation) implies:

$$\frac{\partial \rho}{\partial t} + \vec{\nabla}_{\mathbf{r}} \cdot (\rho \vec{u}) = 0 \quad (2.15)$$

Euler Equation:

The Euler equation (or momentum conservation equation) leads to:

$$\frac{\partial \vec{u}}{\partial t} + \vec{u} \cdot \vec{\nabla}_{\mathbf{r}} \vec{u} = -\frac{1}{\rho} \vec{\nabla}_{\mathbf{r}} P - \vec{\nabla}_{\mathbf{r}} \phi \quad (2.16)$$

Which corresponds to “ $F = ma$ ” for a fluid element.

Poisson Equation:

$$\nabla_{\mathbf{r}}^2 \phi = 4\pi G \rho \quad (2.17)$$

Where the gravitational potential is represented by ϕ .

2.2.2 Perturbation Analysis

We perturb the variables ρ , P , \vec{u} and ϕ producing:

$$\rho \rightarrow \bar{\rho}(t) + \delta\rho \equiv \bar{\rho}(t)(1 + \delta) \quad (2.18)$$

$$P \rightarrow \bar{P}(t) + \delta P \quad (2.19)$$

$$\vec{u} \rightarrow \vec{V} + a(t)H(t)\vec{x} \quad (2.20)$$

$$\phi \rightarrow \bar{\phi}(x, t) + \phi \quad (2.21)$$

We first analyze the continuity equation. We substitute the perturbed variables (2.18) - (2.21) in the continuity equation 2.15:

$$\left(\frac{\partial \bar{\rho}}{\partial t} + 3\bar{\rho}H\right) + \left[\left(\frac{\partial \bar{\rho}}{\partial t} + 3\bar{\rho}H\right)\delta + \bar{\rho}\frac{\partial \delta}{\partial t} + \frac{\bar{\rho}}{a}\vec{\nabla}_x \cdot \vec{V}\right] + \left[\frac{\bar{\rho}}{a}(\vec{V} \cdot \vec{\nabla}_x \delta + \delta(\vec{\nabla}_x \cdot \vec{V}))\right] = 0 \quad (2.22)$$

We take into account only first order terms, so we eliminate the last one. The term between parenthesis describes the background dynamics, given by the Friedmann equation. To obtain them we have to consider again the continuity equation and the Hubble law given by $\vec{u} = H(t)\vec{r}$.

$$\frac{\partial \rho}{\partial t} + \vec{\nabla}_r \cdot (\rho \vec{u}) = \frac{\partial \rho}{\partial t} + \vec{\nabla}_r \cdot (\rho H(t)\vec{r}) = 0 \quad (2.23)$$

Then we have:

$$\frac{\partial \rho}{\partial t} + 3\rho H = 0 \quad (2.24)$$

All the terms between parenthesis in equation (2.22) are null, so the perturbation is given by:

$$\frac{\partial \delta}{\partial t} + \frac{1}{a}\vec{\nabla}_x \cdot \vec{V} = 0 \quad (2.25)$$

Let's do the same thing for Poisson and Euler equations.

For the Euler equation we have:

$$\left(\frac{\partial H}{\partial t} + H^2 + \frac{4\pi}{3}G\bar{\rho}\right)\vec{r} + \left(\frac{\partial \vec{V}}{\partial t} + H\vec{V}\right) + \frac{1}{a}(\vec{\nabla} \cdot \vec{V})\vec{V} = -\frac{1}{a\bar{\rho}}\vec{\nabla}_x \delta P - \frac{1}{a}\vec{\nabla}_x \bar{\phi} \quad (2.26)$$

We remove the second order term and the zeroth order term corresponds to the background dynamics, given by

$$\frac{\partial H}{\partial t} + H^2 + \frac{4\pi}{3}G\bar{\rho} = 0 \quad (2.27)$$

We finally have for the Euler equation:

$$\frac{\partial \vec{V}}{\partial t} + H\vec{V} = -\frac{1}{a\bar{\rho}}\vec{\nabla}_x\delta P - \frac{1}{a}\vec{\nabla}_x\bar{\phi} \quad (2.28)$$

Now the Poisson equation. The perturbed equation is:

$$\left(\frac{1}{a^2}\nabla^2\bar{\phi} - 4\pi G\bar{\rho}\right) + \frac{1}{a^2}\nabla^2\phi = 4\pi G\bar{\rho}\delta \quad (2.29)$$

The term between parenthesis corresponds to the background dynamics:

$$\nabla_r^2\phi = 4\pi G\rho \quad (2.30)$$

So

$$\nabla^2\phi = 4\pi Ga^2\bar{\rho}\delta \quad (2.31)$$

We now continue the analysis by deriving the continuity equation in time:

$$\frac{\partial^2\delta}{\partial t^2} - \frac{1}{a}H\vec{\nabla}\cdot\vec{V} + \frac{1}{a}\vec{\nabla}\cdot\left(\frac{\partial\vec{V}}{\partial t}\right) = 0 \quad (2.32)$$

Combining with Euler and Poisson equations we have:

$$\frac{\partial^2\delta}{\partial t^2} - \frac{2}{a}H\vec{\nabla}\cdot\vec{V} - \frac{1}{a^2\bar{\rho}}\nabla^2\delta\rho - \frac{1}{a}\vec{\nabla}_x^2\phi = 0 \Rightarrow \quad (2.33)$$

$$\frac{\partial^2\delta}{\partial t^2} - 2H\frac{\partial\delta}{\partial t} - 4\pi G\bar{\rho} - \frac{1}{a^2\bar{\rho}}\nabla^2\delta P = 0 \quad (2.34)$$

We have achieved equation (2.34) that is the fundamental equation for the growth of

structures in the Newtonian Theory. It shows the general competition between the gravitational attraction (represented by the term $4\pi G\bar{\rho}\delta$) and the pressure support ($\nabla^2\delta P$).

2.3 Solutions

Consider a Barotropic fluid where $P = P(\rho)$,

$$\delta P = \frac{\partial P}{\partial \rho} \cdot \bar{\rho} \delta \quad (2.35)$$

Where c_s is the sound velocity:

$$\frac{\partial P}{\partial \rho} = c_s^2 \quad (2.36)$$

So we have:

$$\delta P = c_s^2 \cdot \bar{\rho} \delta \quad (2.37)$$

Substituting (2.37) in (2.34) and changing to Fourier space:

$$\nabla^2 \longrightarrow -k^2 \quad (2.38)$$

$$\frac{\partial^2 \delta}{\delta t^2} + 2H \frac{\partial \delta}{\partial t} + \left(\frac{c_s^2 k^2}{a^2} - 4\pi G \bar{\rho} \right) \delta = 0 \quad (2.39)$$

Equation (2.39) is the equation for a damped oscillator in an expanding Universe, provided that:

$$\frac{c_s^2 k^2}{a^2} > 4\pi \bar{\rho} \quad (2.40)$$

On the other hand, if

$$\frac{c_s^2 k^2}{a^2} < 4\pi \bar{\rho} \quad (2.41)$$

The system is gravitationally unstable, allowing gravitational collapse to happen.

The proper wavelength is given by the Jeans length (λ_j):

$$\lambda_j \equiv c_s \sqrt{\frac{\pi}{G\bar{\rho}}} \quad (2.42)$$

Perturbations with proper wavelength equal to or above $\frac{2\pi a}{k}$ are gravitationally unstable. On the other hand, if it is below this value, the perturbations simply oscillate.

Fluctuations bigger than the Jeans length do not have enough time to make pressure to dominate on the gravitational collapse.

2.4 Formation of Dark Matter Halos

There is wide evidence that galaxies reside in extended dark matter halos. These halos appear through gravitational instability as we have already described. Density perturbations grow linearly, reach a critical density and collapse into virialized dark matter halos. They continue to grow through matter accretion or merging with other halos to form more massive ones. Since dark matter halos are intrinsically connected with the birth of galaxies, the properties will have a direct link to the mass function of galaxies. Dark matter halos are non-linear objects, therefore more complex to study but we can use a simpler formalism to find the halos mass function, mass distribution of its progenitors, merger rate and clustering properties. This formalism was first introduced by Press e Schechter (1974) and it helps us understand how dark matter halos properties are connected to the cosmological framework.

The evolution of a spherical density perturbation is identical to the Universe evolution with matter density equal to the critical density. We can consider matter inside the sphere is constant.

$$\frac{d^2 r}{dt^2} = -\frac{GM}{r^2} \quad (2.43)$$

Integrating,

$$\dot{r}^2 = \frac{2GM}{r} + C \quad (2.44)$$

The solution is given by:

$$r = A(1 - \cos\theta) \quad (2.45)$$

$$t = B(\theta - \sin\theta), 0 \leq \theta \leq 2\pi \quad (2.46)$$

$$A^3 = GMB^2 \quad (2.47)$$

If we use these equations as a solution to (2.44), we have:

$$C = -\frac{A^2}{B^2} \quad (2.48)$$

C has a value lower than zero, so the system is bounded. Now lets study the behaviour of this system in primordial time of density perturbation.

If the perturbation expands along with the Hubble flow:

$$\theta \longrightarrow 0 \Rightarrow r \longrightarrow A, t \longrightarrow 0 \quad (2.49)$$

We can take the limits from equations (2.46) - (2.47) with $\lim \theta \longrightarrow 0$ and expand the cosine and sine:

$$r = \frac{A\theta^2}{2} \quad (2.50)$$

$$t = \frac{B\theta^3}{6} \quad (2.51)$$

Or

$$r^2 = \frac{9}{2}GMt^2 \quad (2.52)$$

We can associate r^3 with the spherical perturbation volume:

$$r^3 = \frac{3M}{4\pi\rho} \Rightarrow 6\pi G\rho = t^{-2} \quad (2.53)$$

To associate this result with cosmic expansion, we must remember that:

$$H^2 = \frac{8\pi H\rho}{3} \quad (2.54)$$

$$6\pi G\rho = \left(\frac{9}{4}\right) H^2 \Rightarrow \frac{9}{4} H^2 = t^{-2} \quad (2.55)$$

$$(2.56)$$

So,

$$H = \frac{2}{3}t \quad (2.57)$$

In the beginning of the density perturbation evolution the spherical model evolves like a Universe with Ω very close to 1 ($\rho = \rho_c$). As we advance in time, we advance in θ and we need to expand the results in series that results in:

$$r = \frac{A\theta^2}{2(1 - \theta^2/12)} \quad (2.58)$$

$$r = \frac{A}{2} \cdot \left(\frac{6t}{B}\right)^{2/3} \cdot \left[1 \pm \frac{1}{20} \left(\frac{6t}{B}\right)^{2/3}\right] \quad (2.59)$$

$$t = \frac{B\theta^3}{6(1 - \theta^2/20)} \quad (2.60)$$

The initial system mass is:

$$M = \frac{4}{3}\pi\bar{\rho}r^3 \quad (2.61)$$

If density changes as δ grows, the radius must vary to conserve the mass of the system.

$$M = \frac{4\pi}{3} \bar{\rho} r^3 (1 + \delta)(1 + \delta_r)^3 \quad (2.62)$$

Since $M_{initial} = M_{final}$, it implies

$$1 = (1 + \delta)(1 + \delta_r)^3 \quad (2.63)$$

Expanding to first order:

$$\delta \approx -3\delta_r \quad (2.64)$$

$$\delta \approx -3\delta_r = \pm \frac{3}{20} \left(\frac{6t}{B} \right)^{2/3} \quad (2.65)$$

This way, $\delta \propto t^{2/3}$ like it should be in the Linear Theory. We can use (2.65) to quantify some key points in the history of the evolution of dark matter halos. The first point is growing with Hubble expansion. When the self-gravity of the perturbation reaches a maximum expansion we have $\theta = \pi$; i.e.; $r = 2A$ and $t = \pi B$. The final collapse occurs when $\theta = 2\pi$, $r = 0$ and $t = 2B$.

In this way, we can estimate the over-density at two different moments: turnaround and collapse. At turnaround we obtain:

$$\delta_t = \frac{3}{20} \cdot (6\pi)^{2/3} = 1.06 \quad (2.66)$$

On the other hand, at collapse, we have:

$$\delta_c = \frac{3}{20} \cdot (12\pi)^{2/3} = 1.69 \quad (2.67)$$

2.4.1 Virialized Halos

When dark matter collapses gravitationally it does not form a singularity. Instead, it forms bound structures that eventually reach an equilibrium state, called virilization (virial equilibrium).

In the turnaround, kinetic energy is zero and the total energy equals the potential

energy ($E = U$).

Virial Theorem states that in the equilibrium state:

$$U = -2K \quad (2.68)$$

Where U is the potential energy and K is the kinetic energy. So:

$$E = K + U = K - 2K = -K \quad (2.69)$$

$$U = 2E \quad (2.70)$$

So the potential energy is doubled from the turnaround to the virialization time. The turnaround radius is $r = 2A$ so the final radius must be equal to “ A ”. The halo density is:

$$\rho_H = \frac{3M}{4\pi A^3} \quad (2.71)$$

For an Universe with $\Omega = 1$ we know that:

$$\bar{\rho} = (6\pi Gt^2)^{-1} \quad (2.72)$$

and the collapse time is:

$$t = 2\pi B \quad (2.73)$$

This way:

$$\bar{\rho} = (24\pi^3 GB^2)^{-1} \quad (2.74)$$

The super-density is:

$$\delta \approx \frac{\rho_H}{\bar{\rho}} = \frac{72\pi^3 G M B^2}{4\pi A^3} \approx 178 \quad (2.75)$$

A dark matter halo will always have a density approximately around 200 times the cosmic density in the halo formation epoch.

2.5 Press-Schechter Formalism

Baryonic matter falls into dark matter halos giving birth to galaxies. Until now we only described individual halos but Press & Schechter wondered if there was any way to determine the halo mass spectrum from cosmological considerations. Motivated by the work of Oemler (1973), they developed this idea in 1974 (PRESS; SCHECHTER, 1974) and the theory was named after the two researchers. It is an analytical model to the halo mass function evolution.

Imagine we have a collapsing region with mass M . This mass can be connected with a particular comoving length scale (r or k):

$$M = \frac{4\pi}{3} \rho r^3 \quad (2.76)$$

where,

$$k = \frac{2\pi}{r} \quad (2.77)$$

Considering density fluctuations in spheres with mass M , they have a quadratic mean value given by:

$$\sigma_r^2 = \int \frac{k^2 dk}{2\pi^2} P(k) \cdot (W(k))^2 \quad (2.78)$$

Where $P(k)$ is the fluctuation spectrum and $W(k)$ is the window function in the Fourier space.

A direct way to demonstrate the equation (2.78) can be obtained if we start with the density fluctuation in a sphere with radius R given by:

$$\Delta_R = \frac{3}{4\pi R^3} \int_{sphere} \delta(r) d^3r \quad (2.79)$$

Being the main value represented by:

$$\langle \Delta R^2 \rangle = \frac{3}{4\pi R^3} \int_{sphere} \langle \delta(r) \rangle d^3r \quad (2.80)$$

And $\sigma(R) = \langle \Delta R^2 \rangle^{1/2}$.

An important concept is the “filtering” which means that contributions to the density field below a given scale are filtered out. The mathematical way to do this is:

$$\delta_R = \int \delta(t, r - r') W(r', R) d^3r' \quad (2.81)$$

Where the window function W is associated with a comoving length scale R beyond that W is zero. The normalization of W is:

$$4\pi \int W(r, R) r^2 dr = 1 \quad (2.82)$$

Thus the filtered over-density δ_R is the over-density smoothed over a scale R . For the top-hat filter, we have:

$$W(r, R) = \begin{cases} \frac{3}{4\pi R^3}, & \text{if } r \leq R \\ 0, & \text{if } r > R \end{cases} \quad (2.83)$$

Its Fourier transform is:

$$W(k, R) = \frac{3}{(kR)^3} [\sin(kR) - kR \cos(kR)] \quad (2.84)$$

Since the linear over-density has zero mean, we must take into account the second moment

$$\sigma_R^2 = \langle \Delta R^2 \rangle = \left\langle \frac{1}{V} \int d^3r \delta(\mathbf{r}) W(r) \frac{1}{V} \int d^3r' \delta^*(\mathbf{r}') W^*(r') \right\rangle \quad (2.85)$$

$$\sigma_R^2 = \frac{1}{(2\pi)^6 V^2} \int \int \langle \delta(k) \delta^*(k') \rangle W_k W_{k'}^* e^{i(k-k')r} d^3 k d^3 k' \quad (2.86)$$

$$\sigma_R^2 = \frac{1}{(2\pi)^3} \int \frac{P(k) |W(k)|^2}{V^2} d^3 k \quad (2.87)$$

As we have:

$$W_k = \int d^3 r W(r) e^{-ik \cdot r} = \left[\frac{3kR \cos(kR) - 3 \sin(kR)}{(kR)^3} \right] V \quad (2.88)$$

Then, it is straightforward to obtain equation (2.78). However, note that in the above development it is implicit that $\delta(r)$ corresponds to a random field and it is homogeneous and isotropic. Thus, there exists a spectral representation of the field, which means that we can decompose it in Fourier modes $\delta(k)$ and:

$$\langle \delta(k) \delta^*(k') \rangle = (2\pi)^3 \delta_D(k - k') P(k) \quad (2.89)$$

Where $P(k)$ is the power spectrum. For the reader, an exceptional reference to spectral representation is [Adler \(1981\)](#).

The halos form from peaks in the dark matter fluctuations, so only regions with densities $\delta \geq 1.69$ will collapse. The mass fraction is given by the following Gaussian distribution:

$$f(> M) = \frac{1}{\sqrt{2\pi}} \int_{1.69/\sigma}^{\infty} dx e^{-x^2/2} \quad (2.90)$$

Given that $\nu = 1.69/\sigma$, we have:

$$\frac{df}{dM} = \frac{1}{\sqrt{2\pi}} \frac{d}{dM} \left[\int_{\nu}^{\infty} dx e^{-x^2/2} \right] \quad (2.91)$$

$$\frac{df}{dM} = \frac{1}{\sqrt{2\pi}} \frac{d\nu}{dM} e^{-\nu^2/2} \quad (2.92)$$

The numerical density of the halos with mass M is then:

$$\frac{dn}{dM} = \frac{\rho_0}{M} \frac{df}{dM} = \frac{\rho_0}{M} \frac{1}{\sqrt{2\pi}} \frac{d\nu}{dM} e^{-\nu^2/2} \quad (2.93)$$

And

$$\frac{d \log \nu}{d \log M} = \frac{M}{\nu} \frac{d\nu}{dM} \quad (2.94)$$

Substituting (2.94) in (2.93) we have:

$$\frac{dn}{dM} = \frac{\rho_0}{M} \frac{1}{\sqrt{2\pi}} \frac{\nu}{M} \frac{d \log \nu}{d \log M} e^{-\nu^2/2} \quad (2.95)$$

2.6 The Initial Mass Function (IMF) and the Star Formation Rate (SFR)

The fraction of baryons inside structures is given by the following equation:

$$f_b(z) = \frac{\int_{m_{min}}^{m_{max}} f(\sigma) m dm}{\int_0^\infty f(\sigma) m dm} \quad (2.96)$$

The baryon accretion rate is (DAIGNE et al., 2006):

$$a_b(t) = \Omega_b \rho_c \left(\frac{dt}{dz} \right)^{-1} \left| \frac{df_b(z)}{dz} \right| \quad (2.97)$$

With the critical density of the Universe $\rho_c = 3H_o^2/8\pi G$, dt/dz is the age of the Universe related to the redshift and is described by:

$$\frac{dt}{dz} = \frac{9.78 h^{-1} Gyr}{(1+z) \sqrt{\Omega_\Lambda + \Omega_m (1+z)^3}} \quad (2.98)$$

We now need to know the rate at which stars are formed. This value is given by the Birthrate Function that depends on the Star Formation Rate (SFR), time-dependent, and the Initial Mass Function (IMF). The birthrate function is given by:

$$B(m, t) = \Psi(t) \cdot \varphi(m) dm dt \quad (2.99)$$

The Birthrate equation gives the number of stars formed in the mass interval $(m, m + dm)$ and in the time interval $(t, t + dt)$. $\Psi(t)$ is the SFR, a function of time, and $\varphi(m)$ is the IMF that depends only on the mass of the star.

Salpeter (1959) obtained an empirical relation, valid to the solar neighborhood, that shows the IMF is represented by:

$$\varphi(m) \propto m^{-(1+x)} \quad (2.100)$$

Where $x = 1.35$ is the Salpeter exponent. This formula states that the lower the value of x , the more low mass stars are formed and the higher the value of x , the more high mass stars are formed.

The Salpeter Law was derived through the mass distribution of stars in the solar vicinity (~ 20 pc from the Sun) but it was proved to work in much larger (cosmological) scales (PEREIRA; MIRANDA, 2010). It is convenient to normalize the IMF according to the expression:

$$\int_{m_i}^{m_f} m \varphi(m) dm = 1 \quad (2.101)$$

Where m_i is the minimum mass to ignite nuclear fusion processes and m_f is the higher mass a star can have to maintain hydrostatic equilibrium. Once normalized, $\varphi(m)$ can be expressed as:

$$\varphi(m) = A \cdot m^{-(1+X)} \quad (2.102)$$

The SFR describes the rate at which gas is processed into stars inside galaxies, and exhibits a strong dependence on the gas density. The most usually adopted is the

Schmidt (1959) Law and it follows the following relation:

$$\frac{dM_*}{dt} = k.M_g^n \quad (2.103)$$

Where k is a coupling constant, M_g is the gas mass and n defines the specific model family.

The simplest model takes $n = 1$ then:

$$\frac{dM_*}{dt} = k.M_g \Rightarrow [k] = s^{-1} \quad (2.104)$$

And the star formation characteristic time scale is:

$$\tau = \frac{1}{k} \quad (2.105)$$

This equation states that the SFR is proportional to some power of the volume or surface gas density.

Now that we understand better the IMF and SRF we can construct a detailed relation for the birthrate function. First we are going to express the Schmidt Law as a function of the density:

$$\frac{d\rho_*}{dt} = k.\rho_g^n \quad (2.106)$$

Now, combining the Schmidt and the Salpeter Laws, we obtain:

$$\frac{d^3 N(m, t)}{dV dm dt} = \Psi(t).\varphi(m) \quad (2.107)$$

Where,

$$\Psi(t) = \frac{d\rho_*}{dt} = \frac{d^2 M_*}{dV dt} \quad (2.108)$$

On the other hand, the mass ejected from stars can be calculated by:

$$\frac{d^2 M_{ej}}{dV dt} = \int_{m_t}^{m_s} (m - m_r) \Psi(t - \tau_m) \varphi(m) dm \quad (2.109)$$

Where the lower limit of the integral, $m(t)$, is associated to the stellar mass whose lifetime is “t”, m_r is the mass of the remnant. The star formation is taken at the time $(t - \tau_m)$.

In this way, the equation governing the total gas density in the halos is:

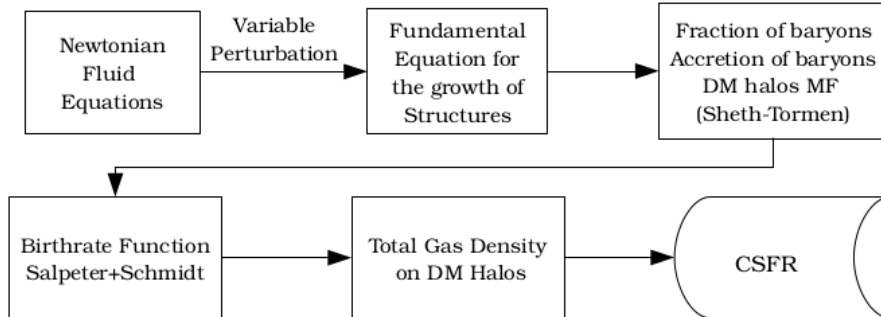
$$\dot{\rho}_g = -\frac{d^2 M_*}{dV dt} + \frac{d^2 M_{ej}}{dV dt} + a_b(t) \quad (2.110)$$

Numerical integration of the above equation produces $\rho_g(t)$. From this parameter we can obtain the cosmic star formation:

$$\dot{\rho}_* = k \rho_g \quad (2.111)$$

In this work, we use results for CSFR developed by [Pereira e Miranda \(2010\)](#) to couple with the Chemical Evolution Model. The simple view of the calculation for the CSFR explained in this section is shown by the following flowchart:

Figure 2.2 - Code



It is important to emphasize that although we use the Press-Schechter formalism, the mass function that describes the halos formed in the redshift z is that derived by Sheth-Tormem, because it presents better results when compared to the computational simulations.

3 ASPECTS RELATED TO THE CHEMICAL ENRICHMENT OF THE UNIVERSE

So far, we understood how large scale structures are constructed in the Universe. Now we have to understand inside the structures, what part of the gas of the Universe formed stars, once they are the players for the chemical evolution. It is in the stars that nucleosynthesis happens and it is because of nucleosynthesis that the Universe is enriched with a lot of elements heavier than H and He, what astrophysicists call “metals”. Chemical evolution models take into account all the variables included in the nucleosynthesis processes and delivers the result of this huge process that happens in the whole universe.

To construct a chemical evolution model from the beginning, we need to take into account several parameters that are essential to the construction of a galaxy. We need to understand the processes behind the production of all elements, the Star Formation Rate and the stellar Initial Mass Function. Also, other than understanding the infall of extragalactic material, radial flows and galactic winds, our model will rely more strongly on understanding the star formation once they are the main components of all galaxies.

We will need to understand how stars are formed, how they evolve while nuclear processes happen inside their cores to produce heavier elements that will later be ejected to the interstellar medium in the form of stellar yields.

3.1 Stellar Evolution and Nucleosynthesis

The phases of stellar evolution and nucleosynthesis are the next very important steps to the model. They are the direct connection between stars and the enriched universe. The mass of the star is what determines which nuclear processes are going to happen in their core and its final fate. We will talk about the mass range, processes and fates of each class of stars and explain in detail nuclear reaction chains, nucleosynthesis processes and the yields.

The chemical elements are formed in nuclear fusion processes that happen inside the hot cores of stars.

According to the mass and metallicity of the star, different processes will take place changing the nucleosynthesis, evolution processes and remnants left behind after they explode in SNe events.

3.1.1 The Evolution of Single Stars

To ignite hydrogen burning, the protostar has to have a minimum mass that implies in a gravitational field strong enough to raise the temperature and pressure in the core in order to start nuclear fusions processes, what also requires quantum tunneling to take place (BALANTEKIN; TAKIGAWA, 1998). For each different mass interval the star will behave differently, according to the nuclear processes that happen in their core and their final fates that will eject (or not) enriched matter to the interstellar medium.

The stellar evolution scenarios can be found in detail in Prialnik (2000) and Kippenhahn (1989) and are summarized in Matteucci (2001) in the following scheme:

- If the star has $M \lesssim 0.08M_{\odot}$, there will never be pressure nor temperature enough to ignite nuclear fusion processes and they would live by producing light from energy liberated through its very slowly contraction along time. These stars have never been observed, and if they exist, they could be able to live several times the age of the Universe.
- For the mass range $0.08 \lesssim M/M_{\odot} \lesssim 0.5$, the star would already be able to reach necessary temperature to ignite H. They keep on burning H into He in the core but when H is exhausted, they are not able to ignite Helium and “die” as white dwarfs. They do not eject material and therefore are not main players in the cosmic chemical evolution.
- A third scenario, when $0.5 \lesssim M/M_{\odot} \lesssim M_{HeF}$, where M_{HeF} is the limiting mass for the formation of an electron-degenerate He-core immediately following the MS (Main Sequence) phase (Its value depends on the treatment of convection but overall it is $\sim 2M_{\odot}$), the star is able to ignite He after H is exhausted and produce Carbon and Oxygen until their end as C-O white dwarfs. They contribute to chemical enrichment by ejecting 4He and ${}^{14}N$ and heavy elements produced by s-processes like Ba and Sr.
- If $M_{HeF} \lesssim M \lesssim M_w$ (where M_w is the limiting mass for the formation of a C-O white dwarf) the star ignites He until it develops an electron degenerate C-O core and ends its life as a C-O white dwarf contributing with the production of ${}^4He, {}^{12}C, {}^{13}C, {}^{14}N, {}^{17}O$, and s-processes elements, produced in the shell.
- In the case where $M_w \lesssim M \lesssim M_{up}$ (where M_{up} is the limiting mass for the formation of an electron degenerate C-O core or the minimum initial mass for an off-center C-ignition proceeding up to central C exhaustion) the stars should burn C in a degenerate core when their mass reaches the Chandrasekhar limit with subsequent supernova explosion. These stars eject the enriched material into the ISM during the AGB phase through mass loss processes. It also goes through episodes of dredge-up

with thermal pulses. The burning envelope then produces ^{13}C and ^{14}N . These stars can also die in the form of SNe Ia contributing to the production of Iron.

- For $M_{up} \lesssim M/M_{\odot} \lesssim 10 - 12$, the contribution for chemical enrichment is given through the production of ^{14}N , ^{12}C and traces of ^{16}O and they would die in the form of type II SNe.
- For $10 - 12 \lesssim M/M_{\odot} \lesssim M_{SNII}$, where M_{SNII} is the limiting mass for the occurrence of a type II Supernova event, the stars are responsible for enriching the ISM with heavy elements such as ^{16}O , ^{20}Ne , ^{24}Mg , ^{28}Si , ^{32}S , ^{40}Ca and r-process elements. They also end as SNe type II and maintain possession of the H-rich core.
- In the case for $M_{SNII} \lesssim M/M_{\odot} \lesssim 100$ we find Wolf-Rayet stars what characterizes a strong mass loss. They contribute to ^4He , ^{12}C , ^{22}Ne , ^{14}N and maybe ^{18}O enrichment.
- When $M > 100M_{\odot}$, the stars either explode as pair-creation SNe, contributing to the production of ^{16}O , or implode as black holes, carrying the enriched material along and not contributing to the ejection of metals in the ISM.
- Last, if $M > 200M_{\odot}$ they produce ^4He and traces of ^{15}N and ^{17}Li when they suffer total disruption by explosive H-burning.

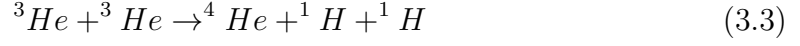
In our preliminary phase of the work, we will be working with stars in the range $0.85 - 260M_{\odot}$, covering great part of the nucleosynthesis processes. The remnant masses can be calculated according to the expressions in Section 3.1.3.

3.1.2 Nucleosynthesis Chains

Once the H core of the star contracts enough to reach about 10 million degrees, nuclear reactions start to happen first transforming Hydrogen atoms in Helium. This high temperature is needed because atoms demand enough energy to cross the Coulomb potential that makes atoms repel each other (RAUSCHER; PATKÓŠ, 2011). These burning processes happen in stages, starting with Hydrogen to produce Helium through the p-p chain and CN cycle.

The reactions in the first branch of the p-p chain are:

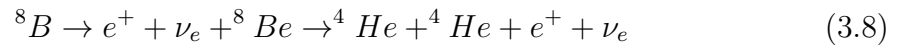




The second branch starts when ${}^3\text{He}$ produced in (3.2) reacts with ${}^4\text{He}$ produced in (3.3):



The third branch of the p-p chain happens when, instead of an electron, a proton is captured by ${}^7\text{Be}$ in (3.5):



When temperatures reach $T > 2.10^7\text{K}$, the CN cycle starts to become more important than the p-p cycle. The reactions in the first branch of the CN cycle are:





When ${}^{16}\text{O}$ is present, the second branch takes place through the following reactions:



The production of helium keeps happening until the hydrogen is exhausted in the core. When that occurs, the interruption of nuclear fusions makes the star undergo a gravitational collapse. If the star is in the according mass range, the core will start contracting until it heats up to temperatures $\sim 10^8\text{K}$. This temperature is high enough to ignite Helium burning. Two ${}^4\text{He}$ atoms fuse together to form ${}^8\text{Be}$, but they decay right away in two ${}^4\text{He}$ atoms again:



The Helium burning then only effective happens when a third part enters the reaction. This process is called the Triple- α reactions:



If the temperatures continue increasing, some other reactions can happen in the Triple- α :



When Helium is exhausted in the stellar core, Carbon burning can be ignited in massive stars ($M > 8M_{\odot}$). The C-O core shrinks until it reaches about $5.10^8 K$. The reactions are:



Or



Neon burning starts at $T = 10^9 K$:



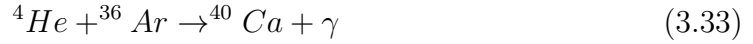
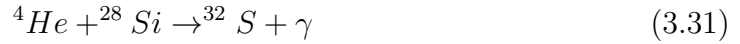
The most important reaction to produce ^{28}Si happens when $T = 2.10^9 K$ and Oxygen burning takes place:



The final stage is ^{28}Si burning, at $T = 5.10^9 K$. At this temperature a series of reactions happen:



The released ^4He build heavier nuclei by successive capture reactions:



And the reactions go on until Iron production. Iron is the heavier element to be produced via nuclear fusion. Instead, the heavier elements are formed through neutron capture processes (r-process or s-process, for rapid and slow, respectively, relative to the time scale of β decay) on the seed nuclei, typically Iron. The slow neutron capture originates very heavy nuclei, completing the elements that cannot be produced via nuclear fusion.

3.1.3 Remnants

The remnant mass can be calculated according to the mass of the star (COPI, 1997):

- For $1M_{\odot} < M \lesssim 8M_{\odot}$, remnant is a C-O White dwarf with mass:

$$m_r = 0.1156m + 0.4551 \quad (3.34)$$

- If $8M_{\odot} < M \lesssim 10M_{\odot}$, the remnant is a O-Ne-Mg white dwarf with mass

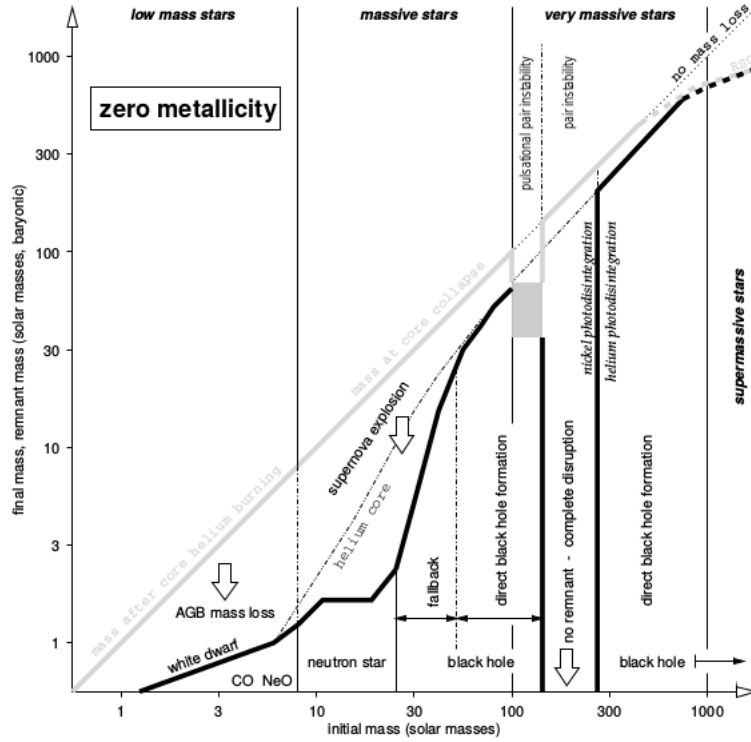
$$m_r = 1.35M_\odot$$

- Stars in the interval $10M_\odot < M \lesssim 25M_\odot$ end as neutron stars with $m_r = 1.4M_\odot$
- If $25M_\odot < M \lesssim 140M_\odot$, the remnant is a black hole and

$$m_r = m_{He} = \frac{13}{24}(m - 20M_\odot) \quad (3.35)$$

Note that stars with $M < 1M_\odot$ and with $M > 140M_\odot$ do not leave any remnants as seen in 3.1. These higher mass stars are the most important metal enrichers from Pop III. The remnants of this Pop III stars and also lower mass Primordial Stars are defined in Fig. 3.1 taken from Heger e Woosley (2002).

Figure 3.1 - Remnants in the Heger e Woosley (2002) for Pop III stars.



3.1.4 Stellar Yields

The stellar yields are defined as the masses of chemical elements produced by stars of different masses (MATTEUCCI, 2016b). We use the stellar yields to determine the elements that were ejected to the ISM at a given epoch. The yields are calculated

through details nucleosynthesis computational simulations, taking into account the main reactions that happen inside the stars, as seen in 3.1.2. Stellar yields used in the model are defined in 4.1.

3.2 Chemical Evolution Models

The first Chemical Evolution Models for galaxies were first developed by Richard Larson and Beatrice Tinsley (TINSLEY; LARSON, 1978), (LARSON et al., 1980).

These models are simple but are the base to all the models we have today. They consider a “galaxy” formed only by gas in a primordial time $t=0$ and the galaxy evolves with time following a law that explains the conversion of the gas into stars. Each formed star then has a chemical production vector, or “yields”, according to the mass.

$$\frac{d}{dt}(gZ) = e_Z - Z\psi + Z_F F - Z_E E \quad (3.36)$$

Where g is the gas mass, Z is the abundance of the specific element, F is the matter infall term and E is the mass outflow and ψ is the star formation rate per mass.

We have developed a chemical evolution model that works coupled to the hierarchical scenario of structure formation developed by Pereira e Miranda (2010). In particular, the production of the chemical element “ y_i ” that is ejected into the environment at a time “ t ” is given by:

$$y_i(t) = \int_{m(t)}^{m_U} [(m - m_R)Z_i(t - \tau_m) + P_{Zm}] \Psi(t - \tau_m) \varphi(m) dm - Z_i \Psi(t) \quad (3.37)$$

where m_R is the remnant mass, P_{Zm} is the element production in a star of mass m , τ_m is the lifetime of a star with initial mass m_i . $Z_i(t - \tau_m)$ takes into account that part of the metals available when the star was formed retained in the remnant. The term $-Z_i \Psi(t)$ takes into account the incorporation of the metals due to a new star generation.

It is important to note that although equation 3.36 has been represented with all terms, we do not take into account the last term, represented as $Z_E E$. This happens because our model is not a hydrodynamical model, what makes a realistic estimate

of this term very difficult. On the other hand, the second-last term in 3.36, $Z_F F$ takes into account the accretion of baryons as discussed in Chapter 2, in particular, equation 2.97.

3.3 Transition from Population III to Population II Stars

3.3.1 Population III Stars

Population III stars (Pop III, also called First Stars or Primordial Stars) is the name given for the very first stars to be formed in the Universe. They were formed from the infall of primordial gas inside dark matter halos, as discussed in the first chapter. They were formed in an environment where the gas was free of heavy elements and therefore they were completely metal free ($Z = 0$), i.e. they would have, in the main sequence, only Hydrogen and Helium.

The cooling of the gas is what makes it fragment and later collapse into a star. Heavy elements, or metals, are the main ingredients for radiative cooling to take place in the gas. Due to the lack of metals, fragmentation of the gas in the early Universe happened very slowly and without fragmentation of the gas clouds into multiple objects - what led to Pop III having high masses from around 30 to 300 Solar masses (SMITH, 2007). Some authors defend the possibility of them having even higher masses, up to 1000 Solar Masses (OHKUBO et al., 2006).

Primordial gas cools and virializes at around $1000K$ inside the halos. H_2 cools the gas to $200K$ and after accumulating the right amount of mass, gravitational collapse takes place. In the literature, we can find studies about the role of each metal in the gas cooling processes. Bromm e Loeb (2003) find that under the temperature and density conditions that characterize population III star formation, the most important coolants are O and C. Other authors consider Fe and Si as important coolants too (SANTORO; SHULL, 2006). But it all depends on the mass range of the first stars, once Pop III with $M > 140M_\odot$ eject large amounts of O, Si, and Fe and stars in the range from 10 to $100M_\odot$ produce smaller amounts of Fe but considerable amounts of α -elements such as O, Ne, Si, S, and Ar (HEGER; WOOSLEY, 2002; HEGER; WOOSLEY, 2010). The importance of these processes is also discussed in 4.3, where we relate these properties to the results in the model developed for this work.

Because Pop III were so massive compared to Pop II, they would also live very short lives. They quickly consumed all the Hydrogen and Helium in their cores, producing large amounts of heavy elements (up to Iron) and dying as Pair-Instability Supernovae (PISNe). Because they had such high masses and no metals, physical

properties and nucleosynthesis processes were different than those of Pop II stars. Pop III were also much more effective at producing ionizing radiation, being able to reionize the Universe early at $z < 17$, as required by the recent detection of large-scale polarization anisotropies in the cosmic microwave background (see Bromm e Loeb (2003)).

In the literature, Pop III stars are found to be divided in the following categories (O'SHEA et al., 2008):

- Population III.1: Stars with only H and He when in the MS (Main Sequence).
- Population III.2: Stars with a very small fraction of metals, but so small that can still be considered $Z \approx 0$
- Population II.5: Transition class between Pop III and Pop II stars.

Pop III stars have never been observed. A series of surveys have been made to find the most metal-poor stars on the Halo of the Galaxy (AOKI et al., 2015; FREBEL; NORRIS, 2015) and, recently, the work of Caffau et al. (2016) have found a star with $Z 10^{-7} Z_{\odot}$. Cai et al. (2011), Cai et al. (2015) explored the possibility of finding Pop III stars through He II $\lambda 1640$ emission lines, which can arise from highly energetic ionizing photons associated with hot metal free stars (CAI et al., 2011; CAI et al., 2015). Also, recent observations of the galaxy CR7 show no metal-lines and also He 1640Å emission lines in its spectrum (SOBRAL et al., 2015), triggering discussions in the literature that maybe pristine gas or zero metal stars could still exist on redshift $z = 6.6$.

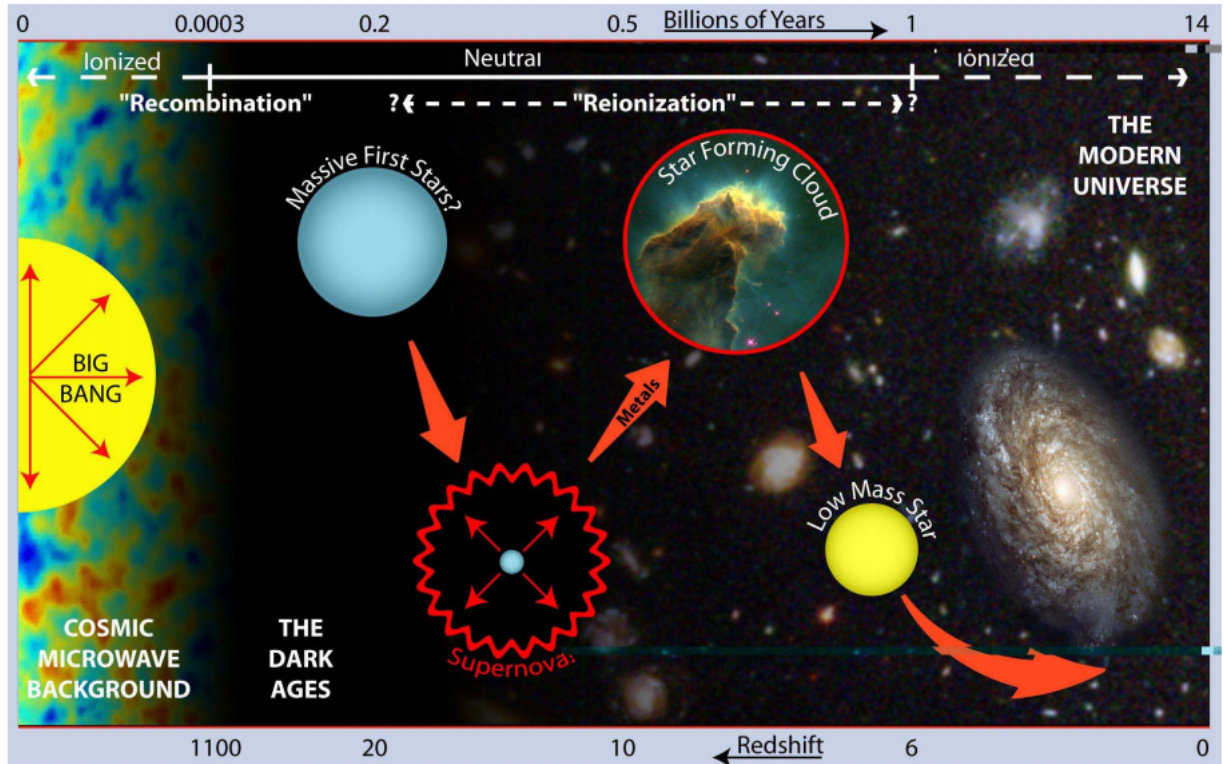
These stars have been simulated in the works of (HEGER; WOOSLEY, 2002, 2002; CAMPBELL; LATTANZIO, 2008) and the chemical yields are used in this work.

3.3.2 Transition and Critical Metallicity

Pop III stars had very high masses being able to quickly ignite nuclear processes in their cores, producing heavy elements from Helium to Iron. They had very short lives (a few Myr) and the chemical enrichment of the Universe began very rapidly as they died as PISNe ejecting their whole greatly enriched masses into the IGM. Pristine gas was quickly enriched by heavy elements, and the increasing of the metallicity made the cooling processes of the gas way more efficient, providing properties for

the second generation of stars to appear. However, the right amount needed for this transition to take place is still inaccurate.

Figure 3.2 - Schematic view of the transition between Populations (National Science Foundation and NASA)



The value of this transition metallicity, or Critical Metallicity (Z_{cr}) is discussed to be between 10^{-6} and $10^{-3}Z_{\odot}$ (see Schneider (2010), Maio et al. (2010), Tornatore et al. (2007a), Fang e Cen (2004), Santoro e Shull (2006)). A series of approaches for the calculations appear on the literature (see, e.g., Smith (2007)). Also, Z_{cr} is thought to be driven mainly by the amounts of Oxygen and Carbon in the medium (FANG; CEN, 2004).

However, the main part of these models take into account one-zone models, and are unable to conclusive evidence of the value for the Transition Metallicity. In this work, we propose that the Transition is indeed driven by the Total Metallicity of the Universe using the results from the semi-analytical model developed to study Cosmic Chemical Evolution.

3.4 Damped Lyman- α Systems - Observational Data

3.4.1 Properties of Damped Lyman- α Systems

In order to test the precision and quality of our theoretical model, we compare our results with observational data from Damped Lyman- α Systems (DLAs).

DLA's are high column density gaseous systems detected through their absorption lines in the optical spectra of quasars ¹. These gaseous systems can be observed up to relatively high redshifts ($z \sim 5$) (HOU et al., 2001). They are selected for the presence of HI column densities ($N_{HI} \geq 2 \times 10^{20} \text{cm}^{-2}$) and Hydrogen is almost completely neutral in DLAs (while it is mostly ionized in other types of QSO absorption systems). They also dominate the neutral gas content of the Universe in the redshift interval $z = [0, 5]$.

We know stars are unlikely to form from ionized gas and are actually more likely to form in cold neutral clouds (WOLFIRE et al., 2003). That makes DLA's the neutral gas reservoir for star formation and they are the regions where star forms from gas that was enriched along the evolution of the Universe. Therefore, understanding its chemical abundances is a key to understanding the chemical evolution of galaxies. The element abundances of DLA's are the most accurate measurements of chemical enrichment of gas at the high-redshift Universe (WOLFE et al., 2005).

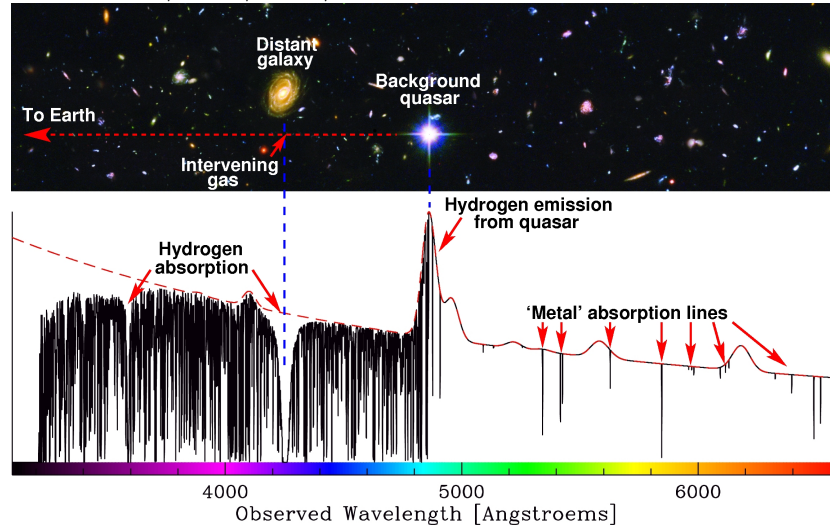
These systems are called Damped Lyman- α Systems because the emission lines we see in the spectrum are within the Lyman- α Forest. The Lyman series of spectral lines are produced by electrons transitioning between the ground state and higher energy levels. Specifically, the Lyman- α transition corresponds to an electron transitioning between the ground state ($n=1$) and the first excited state ($n=2$) of the atom (CARROLL; OSTLIE, 2007). Almost all the lines in the Lyman- α Forest correspond to the same atomic transition (at 1215.67 Å, in the ultraviolet wavelength region) (RAUCH, 2000).

The Ly- α Forest is an absorption phenomenon seen in the spectra of high redshift QSOs and galaxies. Its a group of narrow absorption lines observed in the spectra of all QSOs of the Ly- α emission line. Distant QSOs emit light that travels across the Universe, eventually passing through intervening intergalactic gas (in the form of gas clouds, for example). The gas absorbs part of the light from the quasar, changing its spectrum and giving information about the gas clouds' physical and chemical states. So, the quasar gives the light, and the gas cloud, by absorbing part of the light provides detailed information through the spectra. This Lyman- α Forest is the group of hundreds of sharp absorption lines on the QSO spectra, mostly from

¹Column density is the density projected along the line of sight to the quasar

the neutral hydrogen (H I) Lyman- α line. For a neutral hydrogen atom, spectral lines are formed when an electron transitions between energy levels.

Figure 3.3 - The Lyman- α Forest (not redshift corrected) <http://www.hs.uni-hamburg.de/jliske/qsoal/>



Also, at this high column density ($N_{HI} > 10^{19} cm^{-2}$) the radiation is damped because of the internal finite lifetime of the Ly- α transition.

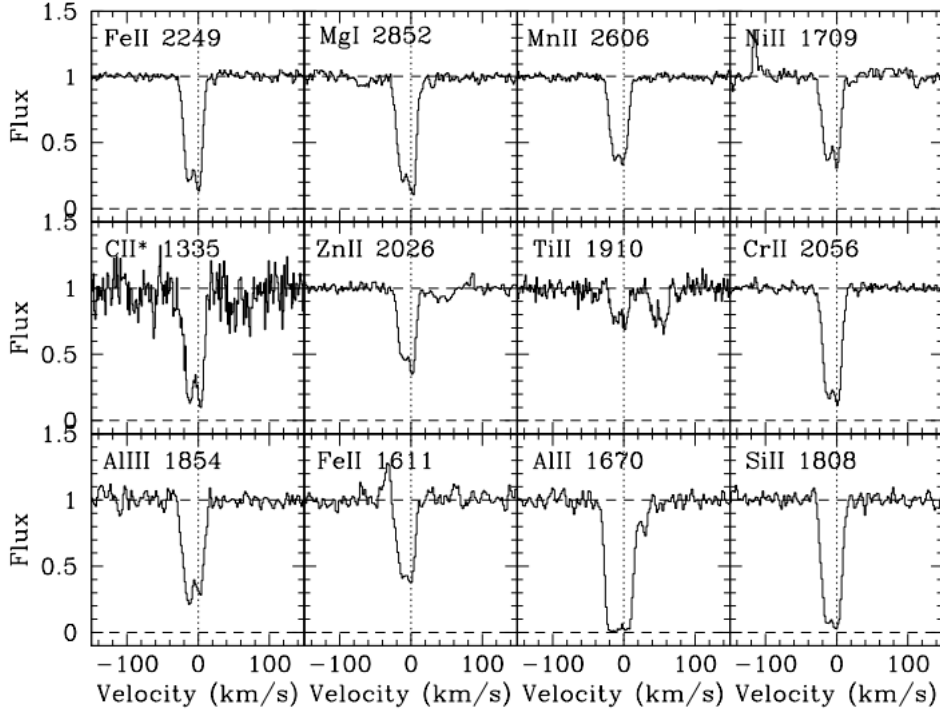
The Hydrogen in DLAs is predominantly neutral due to “Self-shielding”. At high redshifts, part of the gas is commonly high ionized because of UV radiation. However, due to the high density of DLAs, they are “optically thick”, shielding themselves from the ionizing photons and thus remaining neutral. This feature makes it easier for chemical abundance determinations because in the gas phase, heavy elements have a low-ionization potential. The singly ionized elements have an ionization potential of their neutral states lower than the ionization potential of Hydrogen, showing up as dominant spectral features (WOLFE et al., 2005).

Chemical abundances can be determined with a very good accuracy in DLAs, with errors ≤ 0.1 dex or even lower (VLADILLO, 2002). They are inferred using the equivalent width of the absorption lines in the spectra of the DLAs. These equivalent widths are directly proportional to the column density of each metal, so the mass of metals per unit of comoving volume determines the level at which the neutral gas has been enriched.

There can be some problems however with the determination of these abundances: Ionization effects, metallicity radial gradients, outflows, dust darkening, line satura-

tion and dust depletion (VITTI, 2012; NOMOTO et al., 2013), although the last two effects are not important problems for metallicities $\lesssim 0.01Z_{\odot}$. The latter is discussed in 3.4.2. A series of papers have been published featuring chemical abundance data in DLAs. In this work, we use data for chemical abundance of Carbon, Nitrogen, Oxygen, Aluminium, Magnesium, Iron, Zinc, Nickel, Phosphorus and Sulfur.

Figure 3.4 - Metal line transitions in the DLA towards B0105-008. From Ellison et al. (2012)



3.4.2 Depletion

Some fraction of the elements in DLAs can be depleted into dust grains and depletion makes the abundance determination underestimated, i.e., it “hides” part of the metals in the gaseous system. In order to test the depletion patterns, one cannot use the absolute abundance because different DLAs have different metallicities, so absolute ratios are the appropriate tool. As Zn is relatively undepleted in the ISM (with a mean depletion of $[Zn/H] \approx -0.23$) (Savage & Sembach 1996), $[X/Zn]$ ratios are commonly adopted as a measure of depletion.

However, there is not a consensus about the best depletion correction method. A series of different approaches have been used focusing on using the (almost) undepleted elements as reference (see Vladilo (2002)). A good compilation on different

depletion-correction methods possible of using in a work using a similar approach can be seen in [Vitti \(2012\)](#). We compare observed and depletion corrected abundances of Iron and total metallicity with results from our model in [4.3](#) and show that depletion can be important in our model.

4 METHODOLOGY AND RESULTS

4.1 Methodology

This work consists in the Cosmic Chemical Evolution analysis of 11 chemical elements from redshift $z = 20$ ($\sim 180 Myr$) until present. The elements are Oxygen, Iron, Zinc, Nickel, Magnesium, Silicon, Aluminum, Carbon, Nitrogen, Phosphorus and Sulfur.

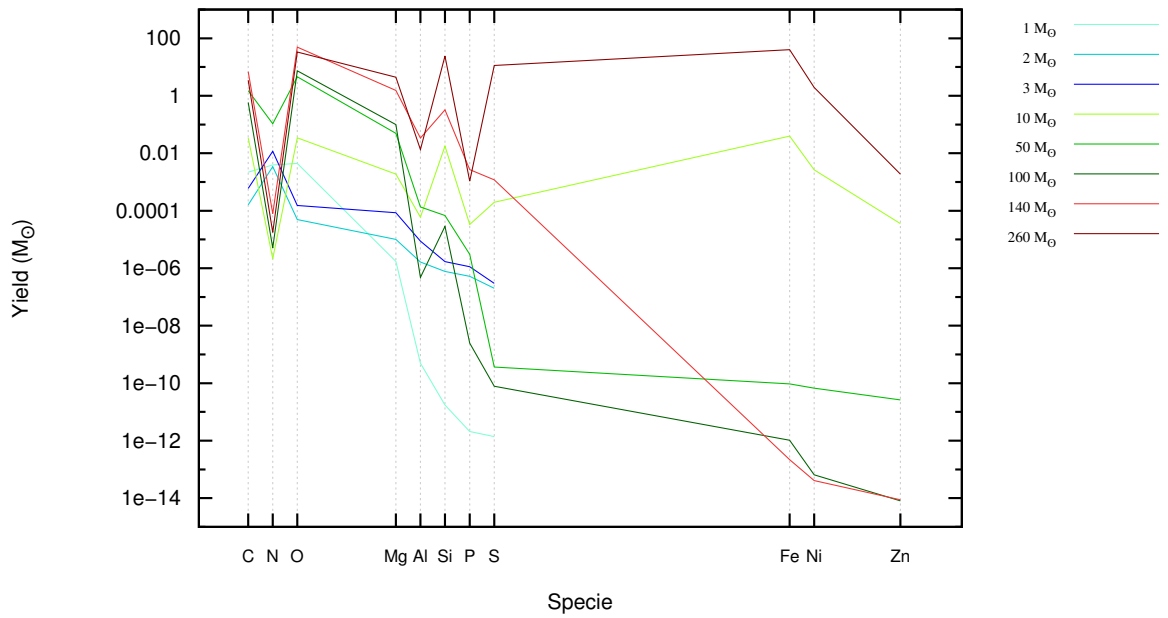
The elements were chosen mainly according to the chemical yields available in the literature and also according to observational data available for chemical abundances in Damped Lyman- α Systems.

We considered yields for Pop III stars from the following works.

- Heger e Woosley (2002), for stars from 140 to 260 M_{\odot} (HW02)
- Heger e Woosley (2010), for stars from 10 to 100 M_{\odot} (HW10)
- Campbell e Lattanzio (2008), for stars from 0.85 to 3 M_{\odot} (CL08)

In the mass range of HW02, stars end their lives as Pair-Instability Supernovae (PISNe), being completely disrupted and ejecting all their matter into the ISM, without leaving any kind of remnants. They are therefore very important objects for chemical evolution in Pop III era. Figure 4.1 it is possible to observe the yields for stars with eight different progenitor masses:

Figure 4.1 - Yields for Pop III Stars according to the progenitor mass.



For Pop II, we chose the following works:

- Chieffi e Limongi (2004), for stars from 13 to 35 M_{\odot} and $Z = 10^{-6}, 10^{-4}, 10^{-3}$ and $2 \cdot 10^{-2}$
- Karakas (2010), for stars from 1 to 6 M_{\odot} and $Z = 10^{-4}, 4 \cdot 10^{-3}, 8 \cdot 10^{-3}$ and $2 \cdot 10^{-2}$
- Doherty et al. (2014a), for stars from 6.5 to 9 M_{\odot} and $Z = 4 \cdot 10^{-3}, 8 \cdot 10^{-3}, 2 \cdot 10^{-2}$
- Doherty et al. (2014b), for stars from 6.5 to 9 M_{\odot} and $Z = 10^{-4}$ and 10^{-3}

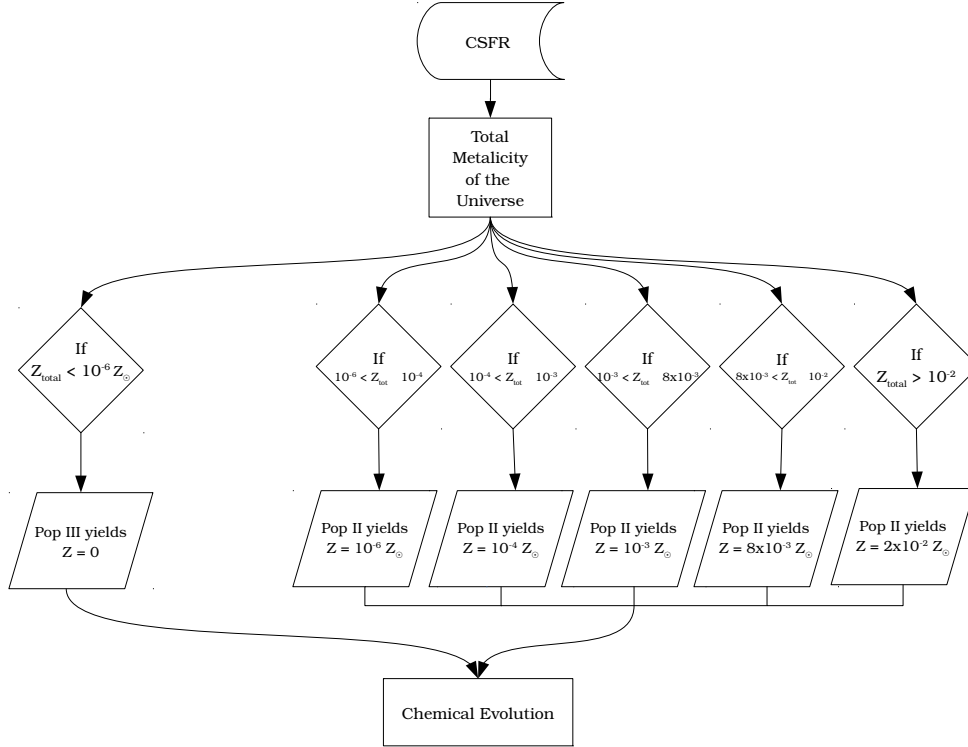
Pop II samples were chosen not only according to the best combination between mass and metallicity range but also according to the models and parameters used to produce each sample. Karakas (2010), Doherty et al. (2014a) and Doherty et al. (2014b) used the MONSTAR code for stellar evolution (FROST; LATTANZIO, 1996), OPAL opacities (IGLESIAS; ROGERS, 1996) and coherent mass loss models (Vassiliadis e Wood (1993), Reimers (1975), Bloeker (1995)).

The calculation is performed in the framework of hierarchical structure formation using a Press-Schechter-like formalism as discussed in Chapter 2, with a Salpeter IMF ($x = 1.35$) and $\tau_s = 2Gyr$ as time-scale for star formation. The code calculates effectively the star formation rate and the results reproduce the observed SFR at redshifts $\lesssim 6.5$. Cosmological parameters used in the code are: $\Omega_m = 0.238$, $\Omega_b = 0.042$, $\Omega_{\Lambda} = 0.762$ and $h = 0.734$. Chemical evolution equations (3.36 and 3.37) were implemented in the code to calculate the enriched eject mass for each star mass range.

The code calculates the Total Metallicity of the Universe (Z_{total}) considering all elements heavier than Helium and not only the 11 selected for this work. The code calculates in parallel the contribution of Pop III stars for the three mass ranges selected. Once Z_{total} reaches $10^{-6}Z_{\odot}$, Pop III stars cease being formed, and the higher mass stars ($\sim 260M_{\odot}$) start dying first, injecting metals into the IGM, according to their specific nucleosynthetic properties. However, the lower mass Pop III stars live longer, and even while stars with much higher metallicities are being formed, these lower mass Pop III stars could still be “alive”, even with the Total Metallicity of the Universe $\sim 10^{-3}Z_{\odot}$, for example. In another way, Pop III stars stop being formed but not to exist and still actively participate in the enrichment of the Universe along with the formation of new, higher-metallicity stars at lower redshifts. Once stars with $10^{-6}Z_{\odot}$ start to exist, the same process happens. Higher mass stars end their

lives first, and even with stars with $10^{-4}Z_{\odot}$ being formed, the lower mass ones keep on existing longer. As the Total Metallicity of the Universe increases, the process keeps on happening until $Z_{total} = 2.10^{-2}Z_{\odot}$. Below, it is possible to see in a simple flowchart scheme the decisions the code makes according to the value of Z_{total} :

Figure 4.2 - Decisions of the code for the Transition between Populations



4.2 Using Damped Lyman- α Systems Chemical Abundances

As discussed in the previous chapter, DLAs are very valuable for studying chemical evolution in the high- z Universe. Chemical abundance determinations in these kind of gaseous nebulae can be determined up to redshift $z \sim 6$ and are the most distant objects with the most accurate chemical abundance measures in the Universe. DLAs are also the perfect site for the initial stages of gas cooling and star formation (MAIO; TESCARI, 2015) and for this reason they provide the best observational data to compare with our model.

We used data from the following works: Centuri3n et al. (1998) (CEN98), Cooke et al. (2011) (C+11), Akerman et al. (2005) (A+05), Dessauges-Zavadsky et al. (2002) (DZ+02), Dessauges-Zavadsky et al. (2003) (DZ+03), Pettini et al. (2008) (PET+08), Pettini et al. (1997) (PET+97), Prochaska et al. (2007) (PRK+07*),

Vladilo (1998) (V97), Nissen et al. (2004) (N+04), Cia et al. (2016) (DC+16) and Kulkarni et al. (2012) (K12).

Solar abundances were different in the majority of the works and were all rescaled for Asplund et al. (2009) solar abundances according to the relation:

$$[X/H]_{DLA_{Rescaled}} = [X/H]_{DLA_{Observed}} + (\log X_{\odot_{Observed}} - \log X_{\odot_{Rescaled}}) \quad (4.1)$$

$$[X/H]_{DLA_{Asplund2009}} = [X/H]_{DLA_{Observed}} + (\log X_{\odot_{Observed}} - \log X_{\odot_{Asplund2009}}) \quad (4.2)$$

Asplund et al. (2009) Solar Abundances are listed in Table 4.1:

Table 4.1 - Element abundances in the present-day solar photosphere from Asplund (2009)

Element	Element abundance
C	8.43 ± 0.05
N	7.83 ± 0.05
O	8.69 ± 0.05
Mg	7.60 ± 0.04
Al	6.45 ± 0.03
Si	7.51 ± 0.03
P	5.41 ± 0.03
S	7.12 ± 0.03
Fe	7.50 ± 0.04
Ni	6.22 ± 0.04

In the case of Vladilo (2002), Pettini et al. (2008), Akerman et al. (2005) and Prochaska et al. (2007) where error is not given, we use a standard error of 0.10 dex. Prochaska et al. (2007) do not show any information about the Solar Abundances used for reference and in that case, the abundance measures were not rescaled and feature a "*" sign on the plots for guidance.

To compare abundances from the model with data from DLAs, it was necessary to use the following relations (see, also, Vitti (2012):

$$[E/H]_{object} = \log[N(E)/N(H)]_{object} - \log[N(E)/N(H)]_{\odot} \quad (4.3)$$

Where $N(E)$ and $N(H)$ are the columnar density for the element E and for Hydrogen, for the object and for the Sun.

In our model, we obtain ρ_{gas} in units of M_{\odot}/Mpc^3 , so:

$$[(E)/N(H)]_{gas} = [\rho(E)/\rho(H)]_{gas} \cdot \frac{M(H)}{M(E)} \quad (4.4)$$

Where $M(H) = 1$

For example, for Oxygen and Zinc:

$$[N(O)/N(H)]_{gas} = [\rho(O)/\rho(H)]_{gas} \cdot \frac{1}{16} \quad (4.5)$$

$$[N(Zn)/N(H)]_{gas} = [\rho(Zn)/\rho(H)]_{gas} \cdot \frac{1}{65.38} \quad (4.6)$$

So,

$$[O/H]_{gas} = \log[N(O)/N(H)]_{gas} - \log[N(O)/N(H)]_{\odot} \quad (4.7)$$

$$[Zn/H]_{gas} = \log[N(Zn)/N(H)]_{gas} - \log[N(Zn)/N(H)]_{\odot} \quad (4.8)$$

By definition, for the Sun, $\log N(H) = 12$:

$$\log[N(O)/N(H)]_{\odot} = \log(O)_{\odot} - 12 \quad (4.9)$$

$$\log[N(Zn)/N(H)]_{\odot} = \log(Zn)_{\odot} - 12 \quad (4.10)$$

We use solar abundance from the work of [Asplund et al. \(2009\)](#) listed in 4.2:

$$\log(O)_{\odot} = 8.69 \quad (4.11)$$

$$\log(Zn)_{\odot} = 4.56 \quad (4.12)$$

So, finally:

$$[O/H]_{gas} = \log[\rho(O)/\rho(H)] \cdot \frac{1}{16} - (8.69 - 12) = \log[\rho(O)/\rho(H)] \cdot \frac{1}{16} + 2.106 \quad (4.13)$$

$$[Zn/H]_{gas} = \log[\rho(Zn)/\rho(H)] \cdot \frac{1}{65.38} - (4.56 - 12) = \log[\rho(O)/\rho(H)] \cdot \frac{1}{65.38} + 7.44 \quad (4.14)$$

Also, data taken from [Cooke et al. \(2013\)](#) provides abundances referent to Iron instead of Hydrogen. We used the relation:

$$[E/Fe] = [E/H] - [Fe/H] \quad (4.15)$$

$$[E/H] = [Fe/H] + [E/Fe] \quad (4.16)$$

In order to test the accuracy of the model with data from DLAs, a value for χ^2 is presented in some cases. It is calculated through the equation:

$$\chi^2 = \sum_{i=1}^N \frac{(y_i - M_i)^2}{\sigma^2} \quad (4.17)$$

Where M_i is the data generated by the model, y_i are the observational data points and σ are the errors associated to them ([BEVINGTON, 2002](#)). It is important to note that the dispersion of DLA data is high in every case, and that, accompanied by the very low errors associated to each measure, delivers very high values for χ^2 . Nevertheless, the results are for comparison between two or more situations where the model can improve the agreement with observational data and therefore the statistical tests are valid.

4.3 Results and Data Discussion

Here we present the data generated in the model. The plots were divided in three curves:

- The red curve considers only Pop III yields from 0.85 to $260M_{\odot}$. It represents the upper limit for metallicity.
- The blue curve is a test running only for Pop II yields, representing the lower limit for metallicity.
- the pink curve is the final model, considering the transition between Pop III and the next more metal rich Population II generations.

The first evidence arising from the plots is the inability of Pop II yields in representing today's metal abundances for almost all the elements studied, with exception of Carbon and Nitrogen only. That means that stars with physical characteristics and nuclear processes as developed in the models in the literature by [Heger e Woosley \(2010\)](#), [Heger e Woosley \(2002\)](#) and [Campbell e Lattanzio \(2008\)](#) for Population III must have existed in the primordial Universe.

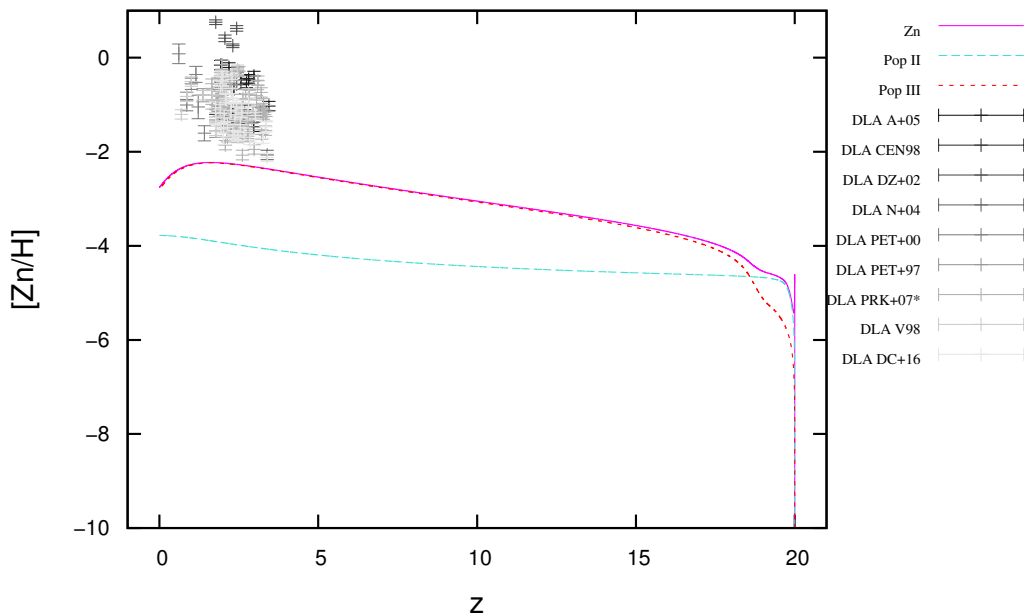
To abridge, Sulfur is the element that shows the better agreement comparing the model with observations. Aluminum, Phosphorus and Magnesium show a good agreement too, but are a little underabundant. Iron and Silicon are a little overabundant. Nickel and Zinc are underabundant and Carbon, Nitrogen and Oxygen show an overabundance, but Oxygen not so much as Carbon and Nitrogen.

4.3.1 The Underabundance of Zinc and Hypernovae Nucleosynthesis

Zinc was studied in a preliminary version of the model considering only Pop III yields in the work developed by Vitti (2012). The model presented an underabundance of Zinc that appears again in our model. Even considering the Transition to Pop II and their respective yields, there is not enough production of Zinc to reach the abundance determinations in DLAs. Zinc is considered to be undepleted in DLAs (it is very commonly used as undepleted reference for measuring depletion in other elements, as seen in 3.4.2) so that is not the problem of the underabundance.

Zinc is mainly produced in Hypernovae (HNe) explosions. HNe are characterized by larger production of Zn , Co , V and Ti than normal SNe; A large explosion energy E enhances α -rich freezeout, which results in the increase of the local mass fractions of Zn and Co (NOMOTO et al., 2006a).

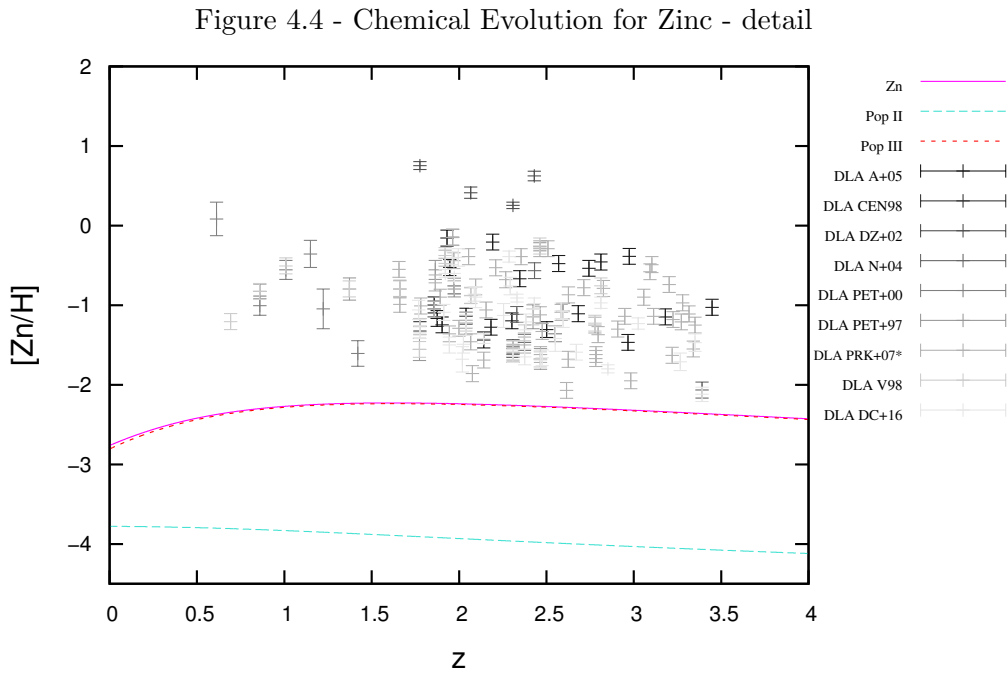
Figure 4.3 - Chemical Evolution for Zinc



HNe explosions produce large quantities of Zinc, providing a food mechanism for enhancing Zinc abundances in the model. Another advantage of considering HNe yields is the Carbon burning process: Hypernovae use Carbon, Oxygen and Aluminum as fuel for producing heavier elements. As Carbon and Oxygen are superabundant in the model, using HNe yields would also help decreasing their abundances.

There are two issues: HNe events use Aluminum as fuel too, which is underabundant in the model, and produces Silicon, which should be a little lower, leaving the question of if HNe are really the best option for inserting Zinc and taking part of the Carbon and Oxygen out.

However, the yields for Aluminum are still positive, meaning that despite it being used as fuel, HNe also ejects it.



Another mechanism would be a higher mass Pop III branch. [Ohkubo et al. \(2006\)](#) developed synthetic yields for stars with 500 and $1000M_{\odot}$. This branch would produce large amounts of Zn compared to O , C and other metals, and could rise Zn abundances without raising O and C too much. In Fig. 4.5 we can see the yields for the two higher mass stars from ([OHKUBO et al., 2006](#)) and in Figure 4.6 there is the comparison between this branch and the other 3 branches considered in the model.

Figure 4.5 - Yields from Pop III for 500 and 1000 M_{\odot} stars (OHKUBO et al., 2006)

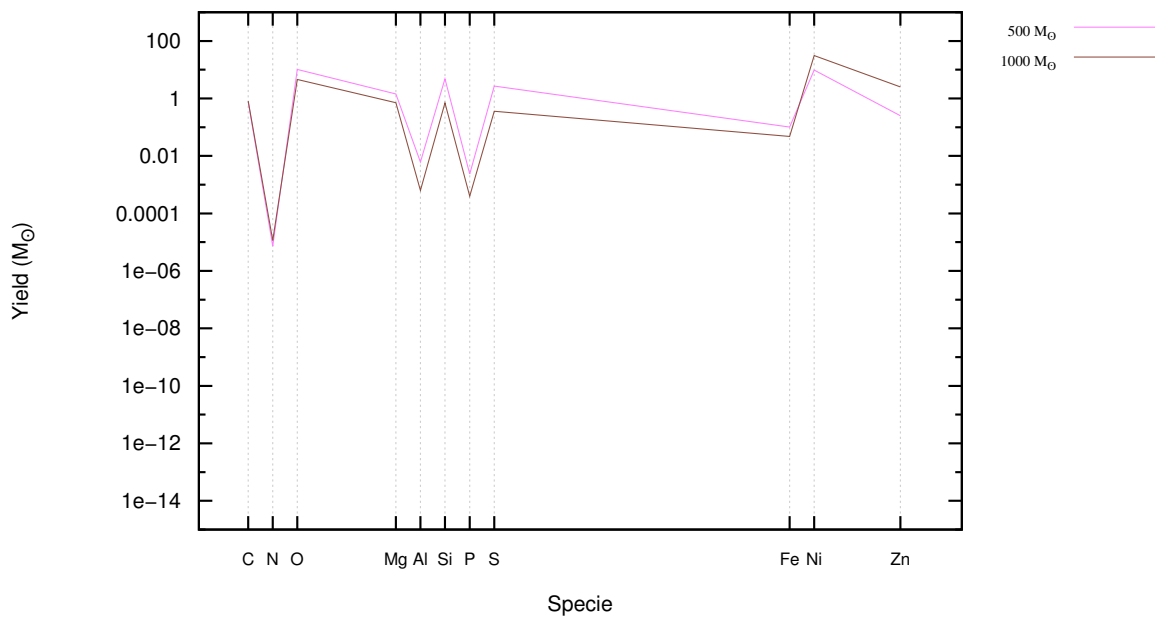
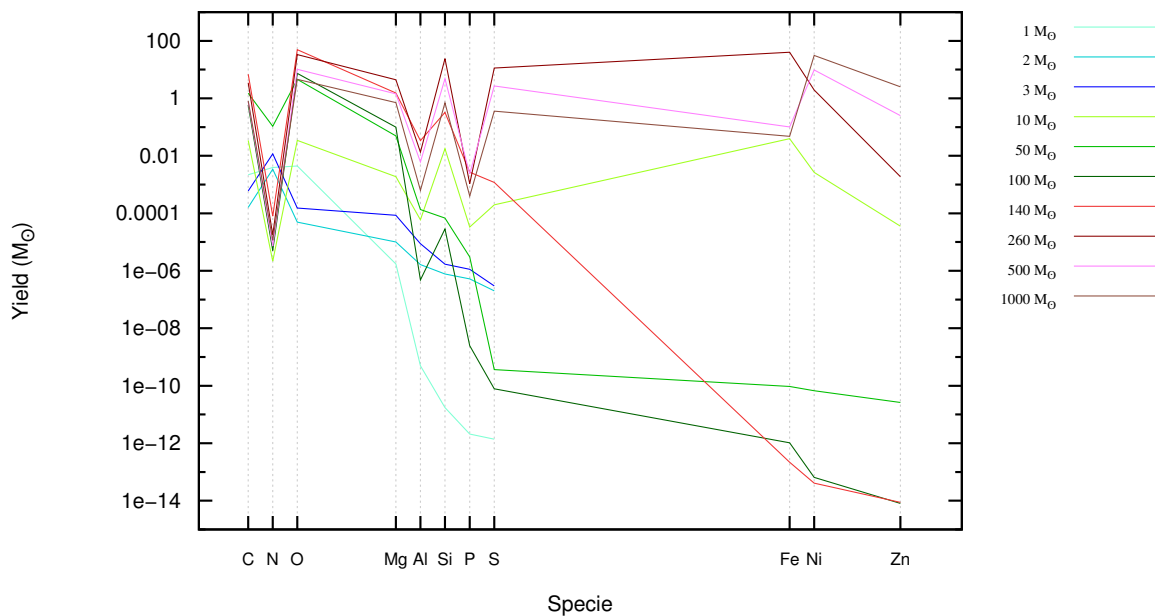


Figure 4.6 - Yields for Pop III original mass branches compared to Ohkubo et al. (2006) yields for 500 and 1000 M_{\odot} stars.



4.3.2 The Underabundance of Aluminum

Aluminum is underabundant in our model compared to data from DLAs. One of the reasons could be the problem in measuring Al in the spectra of DLAs. The Al II $\lambda 1670$ line is the strongest metal line transition observed in the DLA systems (PROCHASKA; WOLFE, 2002). In the majority of systems the line is heavily saturated and, together with blending of lines and blending with the Ly- α Forest, determining Al abundances can be a real challenge. In the work of Dessauges-Zavadsky et al. (2003), in the measure for $z = 3.882$, for example, the Al II $\lambda 1640$ line has to be identified in the middle of a contamination by telluric lines. These lines are identified but some components remain blended, deriving in a large error in the deduction of Al abundance (DESSAUGES-ZAVADSKY et al., 2003). This is one of the higher abundances measured for Aluminum and it should be looked into carefully for relevance - as much as the other determinations. But if we disconsider this measure, Al results improve. A χ^2 analysis, for example, drops from 127.23 to 70.69 if the higher measures are taken out (while χ_{red}^2 drops from 21.20 to 11.78). The refractory nature of Al is not very well determined so it is not possible to accurately know the depletion factors for this element.

Figure 4.7 - Chemical Evolution for Aluminum

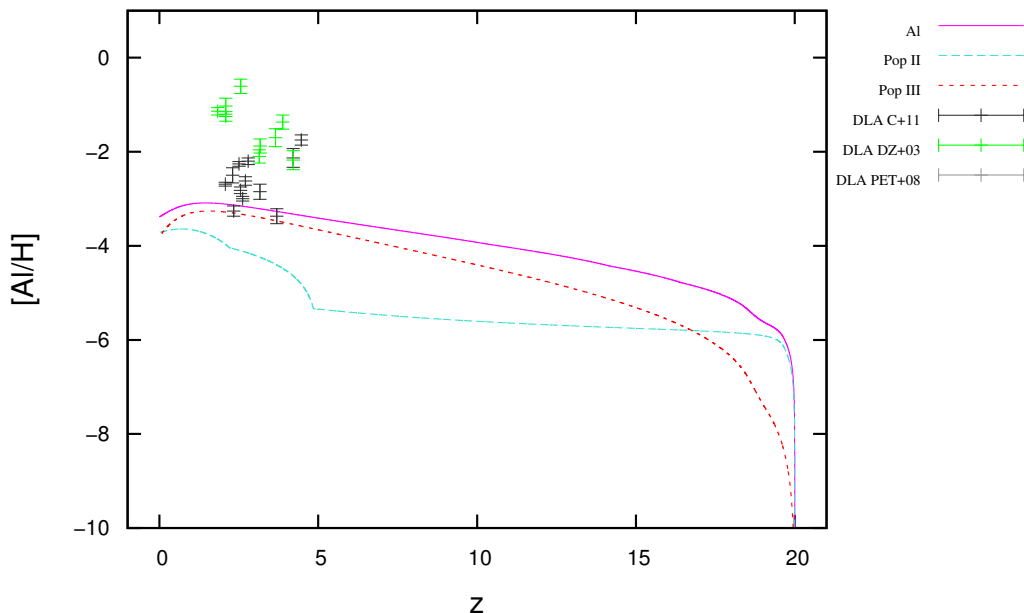
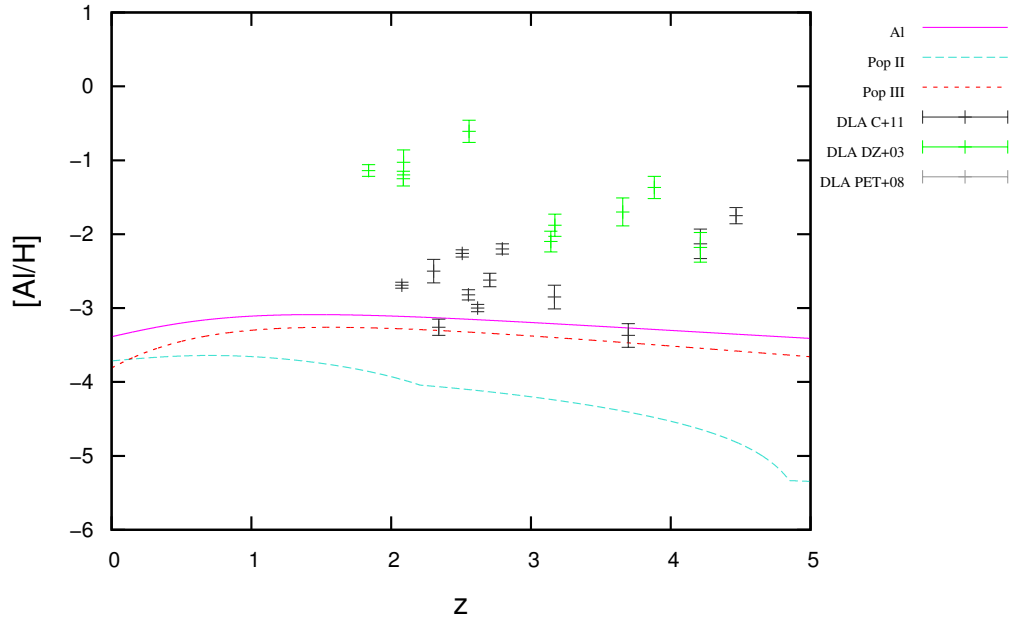


Figure 4.8 - Chemical Evolution for Aluminum - detail



Note: If we disconsider abundance measures taken from DZ+03 because of possible measurement uncertainties, χ^2 improves from 127.23 to 70.69.

4.3.3 Magnesium: Underbundance or DLA Problems?

The element Magnesium appears to be underabundant in the model comparing with the total dispersion of the observational data points. However, if we disconsider the top measures, Mg appears to be very well represented compared with chemical abundances from [Dessauges-Zavadsky et al. \(2003\)](#) [Cia et al. \(2016\)](#). In fact, a careful look into the work of [Dessauges-Zavadsky et al. \(2002\)](#), from where the top two abundances were taken from, reveals a problem with those measures. The author points out that the measures are over-solar contrary to the expected from differential depletion. Despite the effect being in the error bar limits, it is worth investigating because it could be a signature from a peculiar nucleosynthesis effect specifically from the cloud observed. The author suggests that Mn , Ti and Mg are additional elements to compare with and further investigations could lead to a better understanding of the nature of the Star Formation History inside the system. A χ^2 analysis drops from 14.39 to 12.43 (while χ_{red}^2 drops from 2.40 to 2.07) if the top two measures are taken out.

Magnesium is also a refractory element, which means depletion could also be a problem in taking this element abundances. Besides that, another challenges arise from Magnesium determination in this work due to the saturation of the doublet used to determine Mg , leaving one only line possible of providing Mg abundance. This lines are blended with the Ly- α lines. Given all the problems in this determination, they should be confirmed by additional Mg measures to conclude if it could or could not be a particular nucleosynthesis effect ([DESSAUGES-ZAVADSKY et al., 2002](#)).

Figure 4.9 - Chemical Evolution for Magnesium

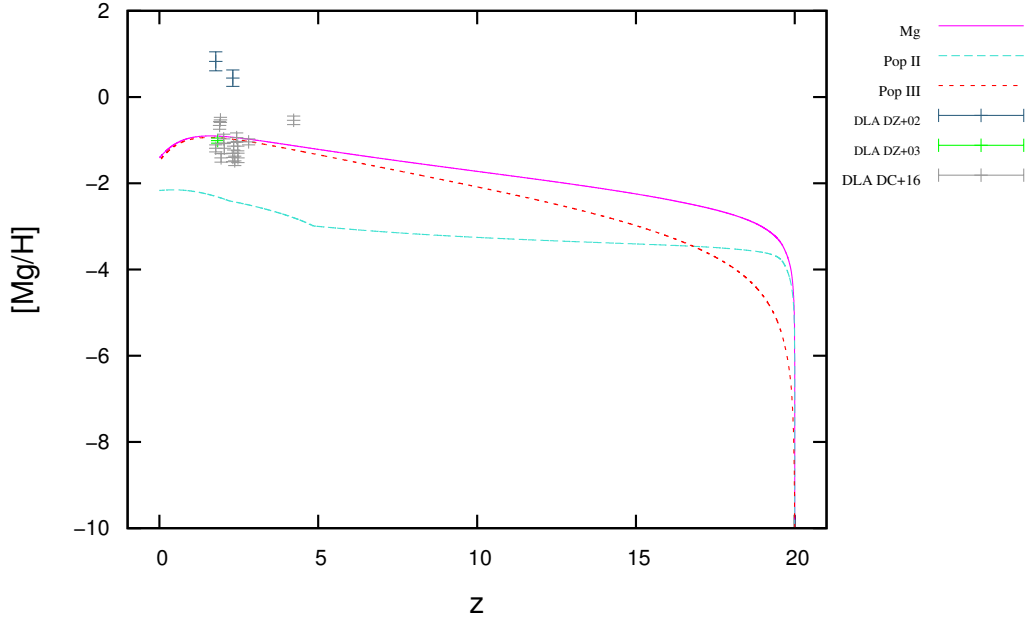
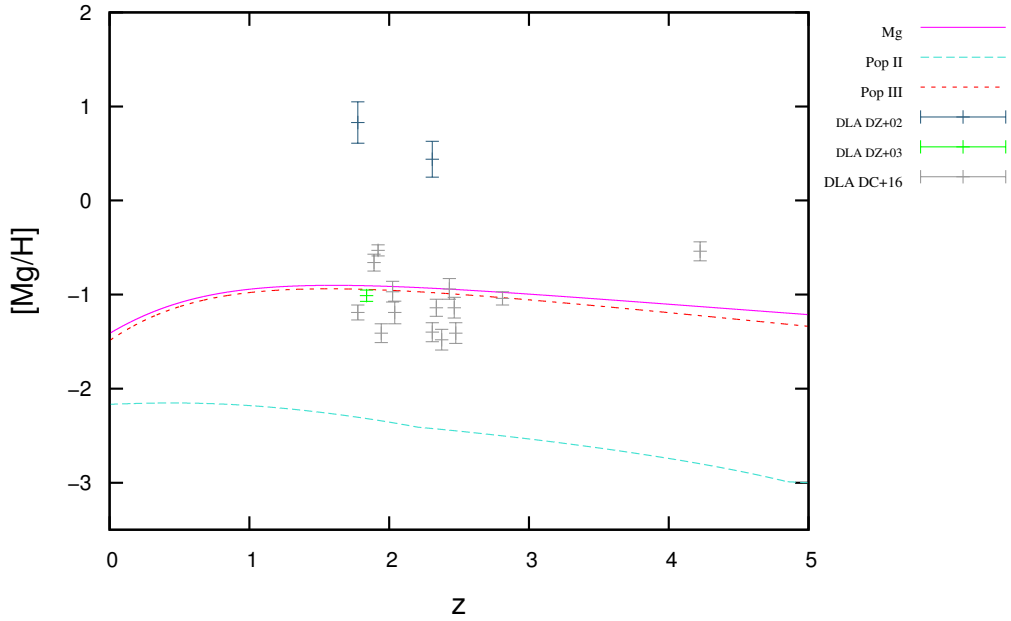


Figure 4.10 - Chemical Evolution for Magnesium - detail



Note: If we disconsider the two higher abundance measures taken from DZ+02, χ^2 improves from 14.39 to 12.43. In fact, the author suggests that those two measures are worth of a deeper investigation once they could be affected by a peculiar signature of nucleosynthetic effects from the specifically cloud observed (DESSAUGES-ZAVADSKY et al., 2002).

4.3.4 The underabundance of Phosphorus and Nickel

Phosphorus and Nickel appear to be a little underabundant in the model. Phosphorus is produced in massive stars via C , O and Ne burning and a large part of ^{31}P is destroyed via (p, α) reactions to become ^{28}Si . (MACIA, 2005; Cescutti et al., 2012). P is also produced in SNe Ia along with Ni . As we see in the results for these two elements (Fig 4.11, 4.12, 4.13 and 4.14), Nickel is more underabundant than Phosphorus and fits better to the model, with $\chi^2_{Ni} = 342$ ($\chi^2_{red,Ni} = 57$) and $\chi^2_P = 97$ ($\chi^2_{red,P} = 16.2$), so, in order for SNe Ia yields to be the best solution for this problem, this phenomenon should yield more Nickel than Phosphorus. In fact, yields proposed by (NOMOTO et al., 1997) show that a SNe Ia explosion ejects between $\sim 4 \times 10^{-3}$ and $1.4 \times 10^{-2} M_{\odot}$ of Ni and from $\sim 8.5 \times 10^{-5}$ to $4 \times 10^{-4} M_{\odot}$ of P (depending on the model - see (NOMOTO et al., 1997)), meaning that including SNe Ia in the model could solve the problem for these two elements as well.

The higher mass branch from Ohkubo et al. (2006) produces little P but higher amounts of Ni (as seen on Figs. 4.5 and 4.6), meaning it would be interesting to consider this mechanism in future versions of the code to solve P and Ni problems.

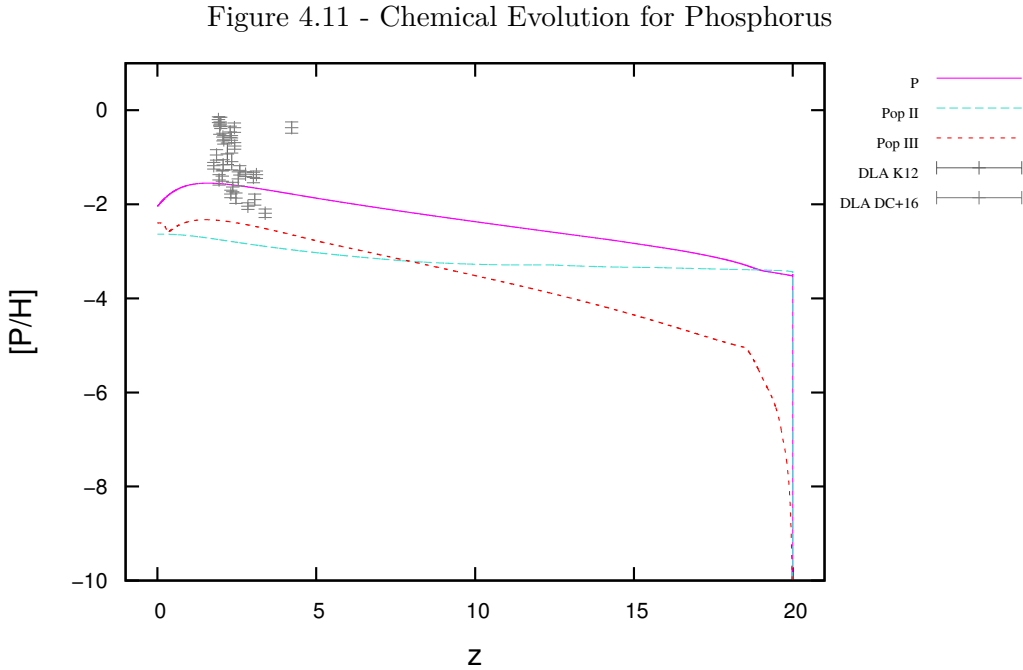


Figure 4.12 - Chemical Evolution for Phosphorus - detail

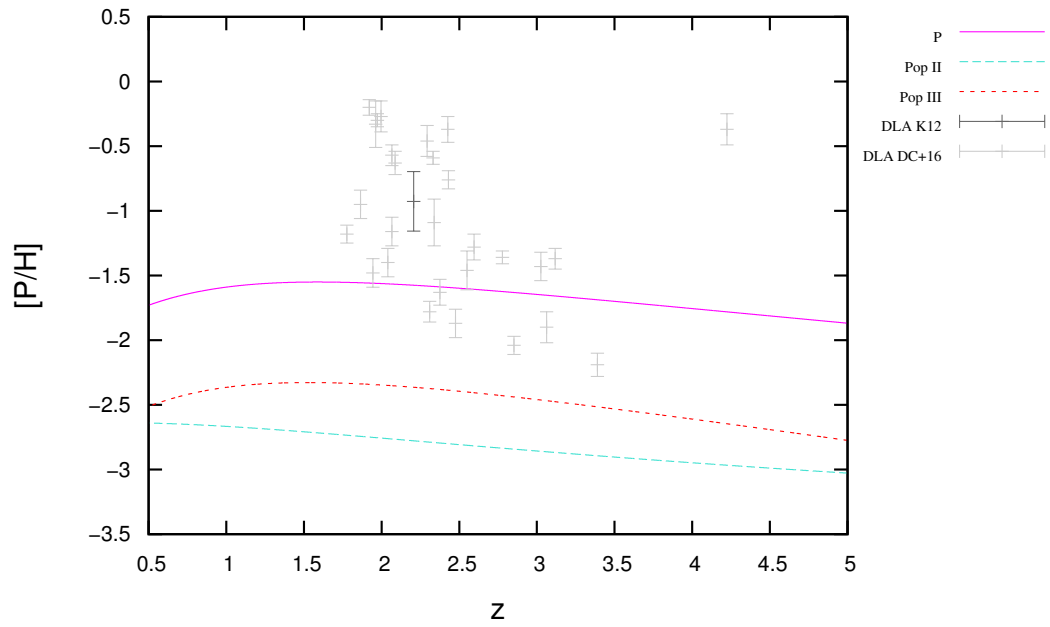


Figure 4.13 - Chemical Evolution for Nickel

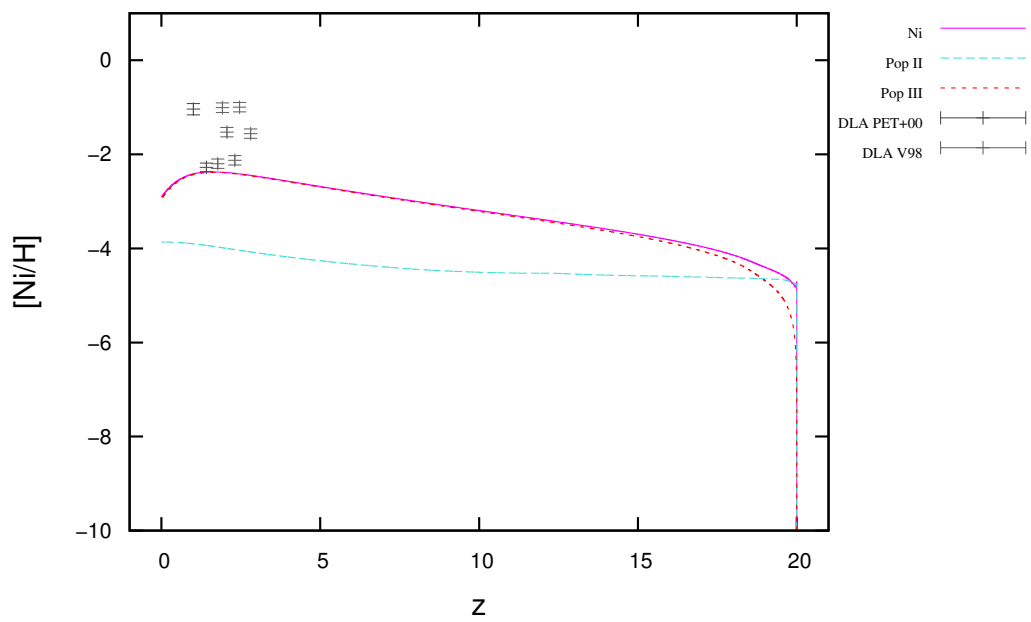
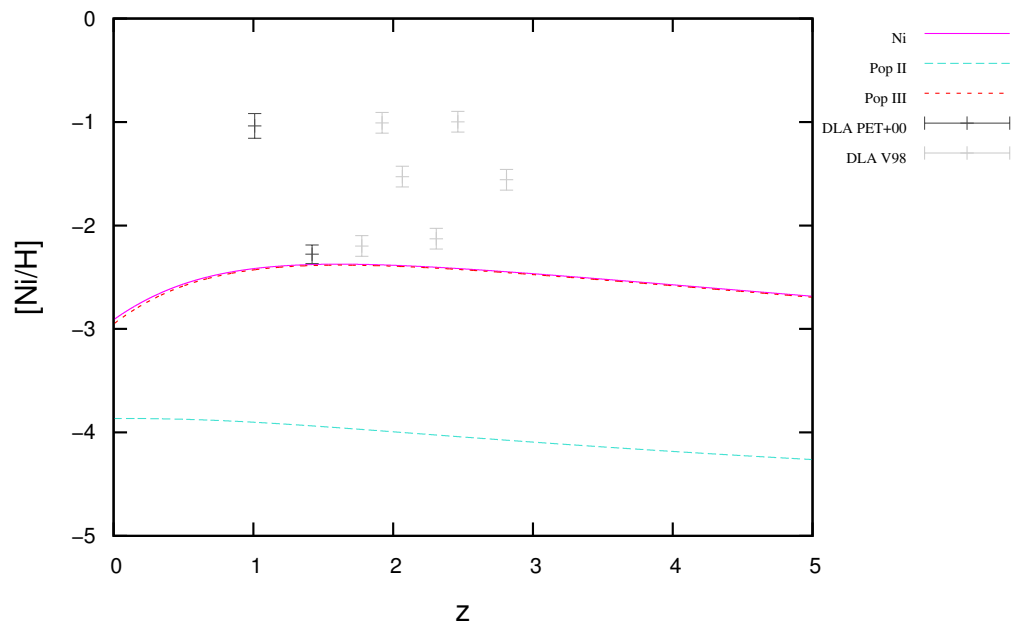


Figure 4.14 - Chemical Evolution for Nickel - detail



4.3.5 The Iron and Silicon Superabundance

The elements Silicon and Iron are a little overabundant in the model. This behaviour is unexpected once both elements are mainly synthesized in SNe Ia and also in HNe, for the case of Silicon.

However, Cia et al. (2013) considers that Fe and Si can be altered by depletion. Depletion “drags” abundances down, once part of these elements are “traped” into dust grains. That way, Fe and Si should show higher abundances, improving the agreement with the model.

We compare data from Vladilo (2002) for Iron depletion-corrected and not corrected with results from our model and the result can be seen in Figs. 4.19 and 4.20. A quick analysis reveals a decrease from $\chi_{obs}^2 = 78.93$ ($\chi_{red,obs}^2 = 13.15$) to $\chi_{corr}^2 = 18.19$ ($\chi_{red,corr}^2 = 3.03$) for observed and dust corrected abundances compared to results in our model, reaffirming the importance on dust depletion for Iron. Details about the methodology used to correct depletion for Iron can be checked on Vladilo (2002).

For Prochaska e Wolfe (2002), although silicon is a refractory element, its depletion is not strong enough to alter significantly the abundances for DLA systems.

Either way, further analysis on depletion should be made to further investigate its effects on Silicon and other metals.

Figure 4.15 - Chemical Evolution for Iron

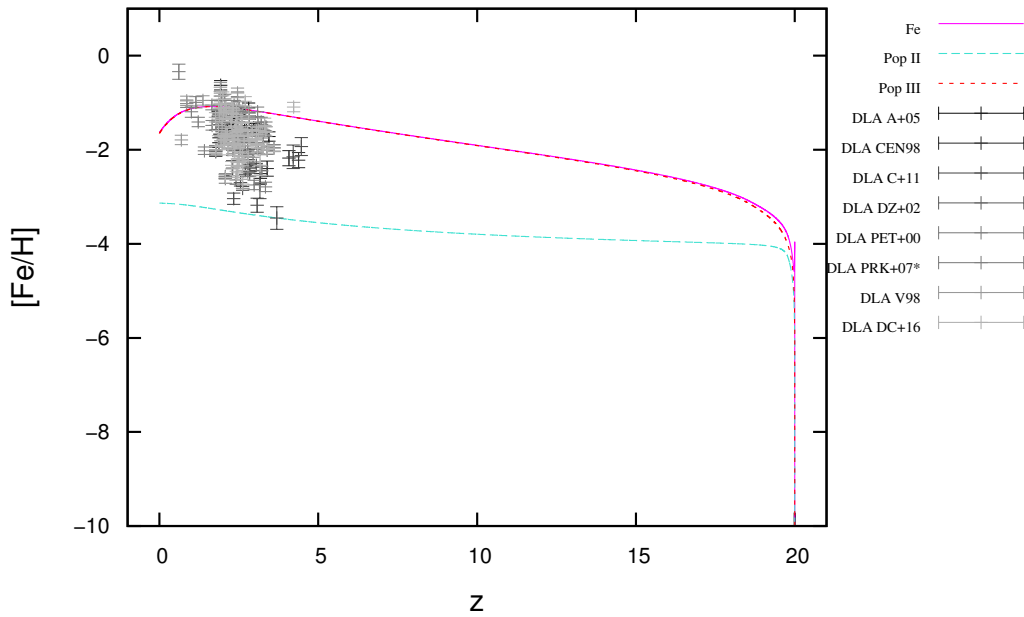


Figure 4.16 - Chemical Evolution for Iron - detail

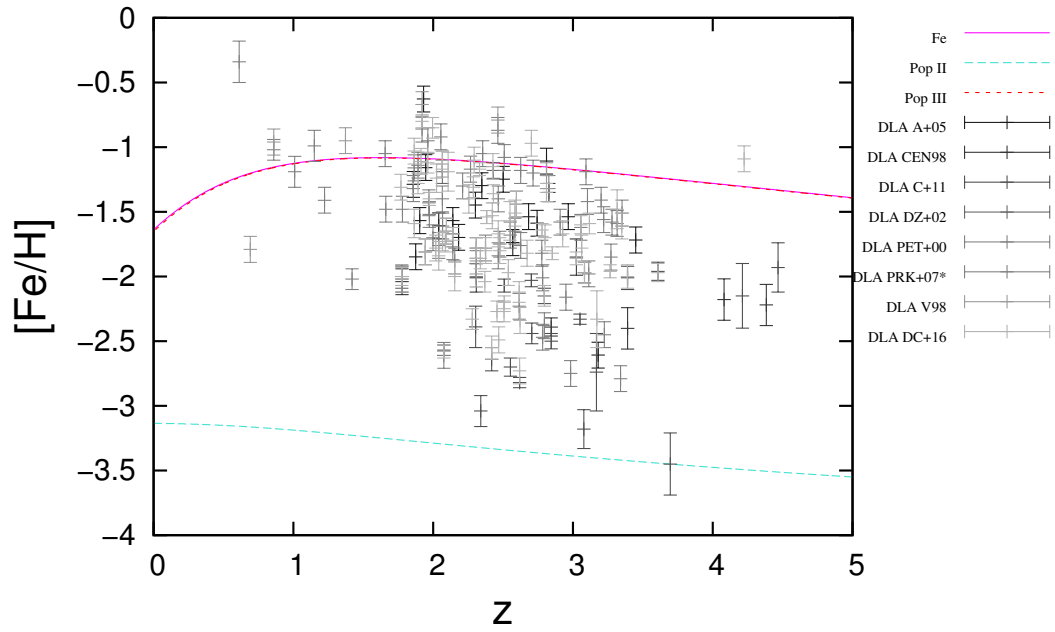


Figure 4.17 - Chemical Evolution for Silicon

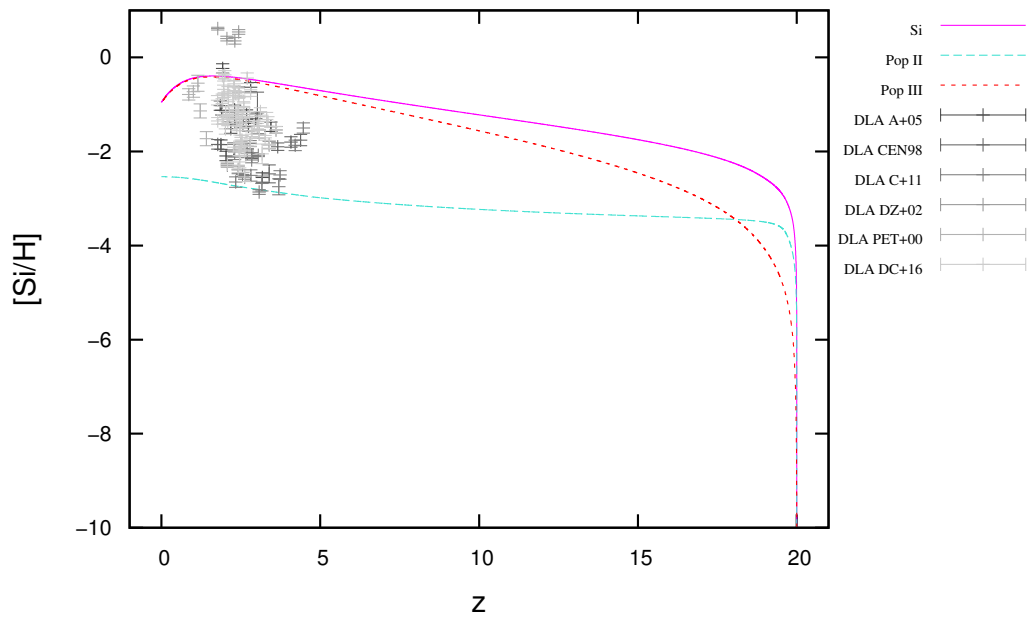
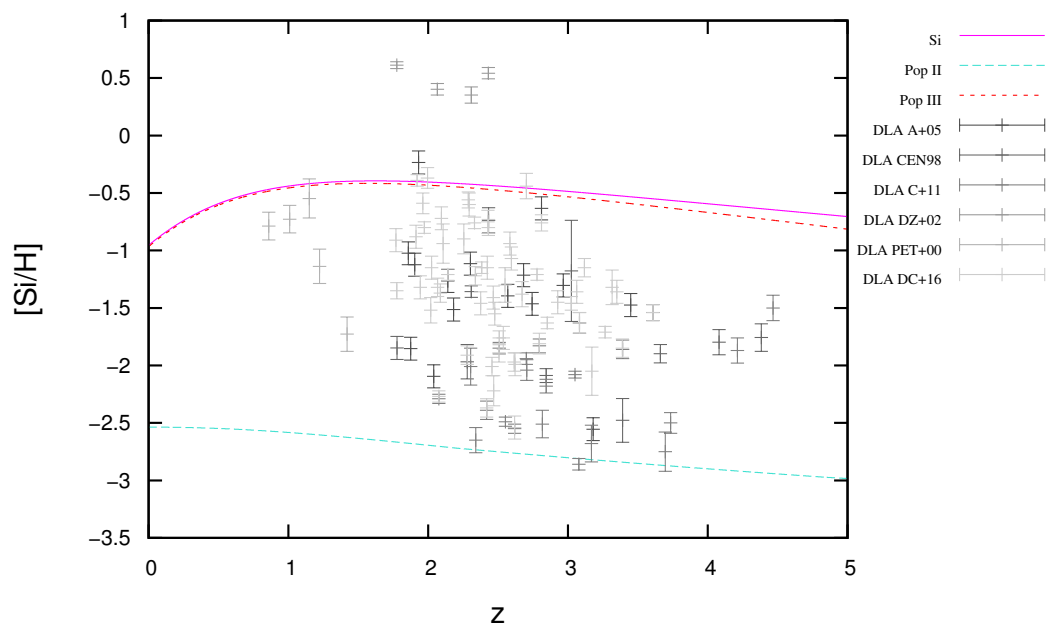


Figure 4.18 - Chemical Evolution for Silicon - detail



The Influence of Depletion:

Figure 4.19 - Depletion of Iron on DLAs

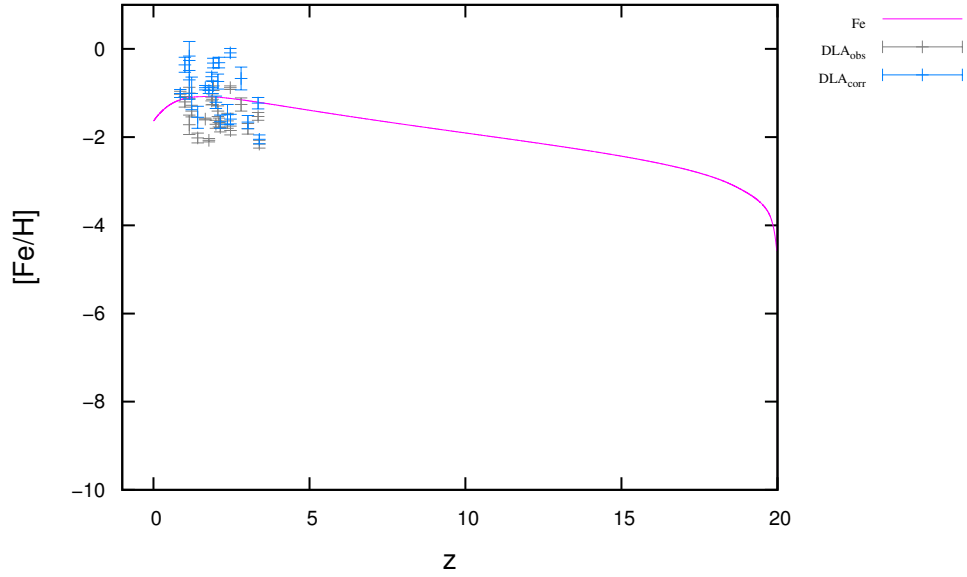
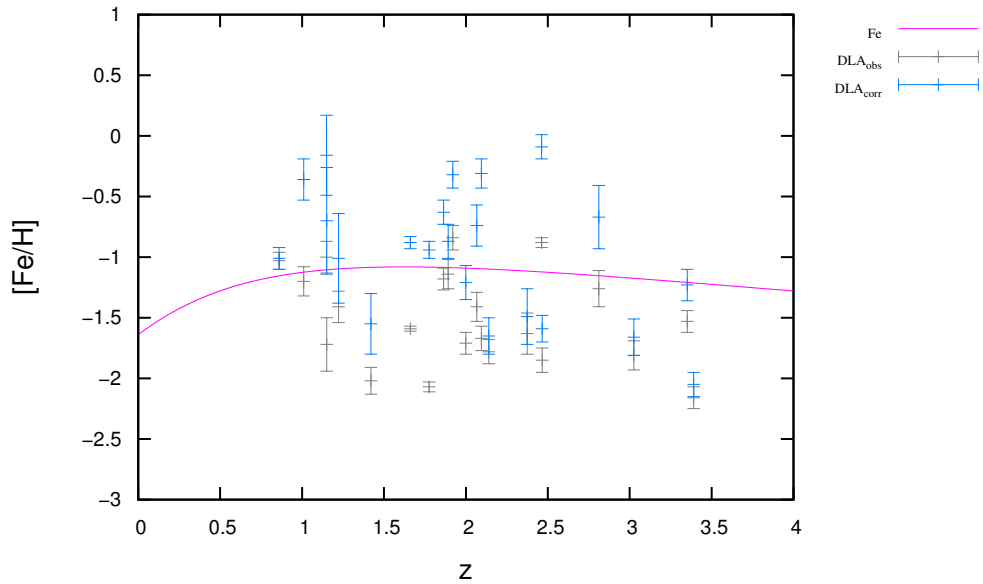


Figure 4.20 - Depletion of Iron on DLAs - Detail

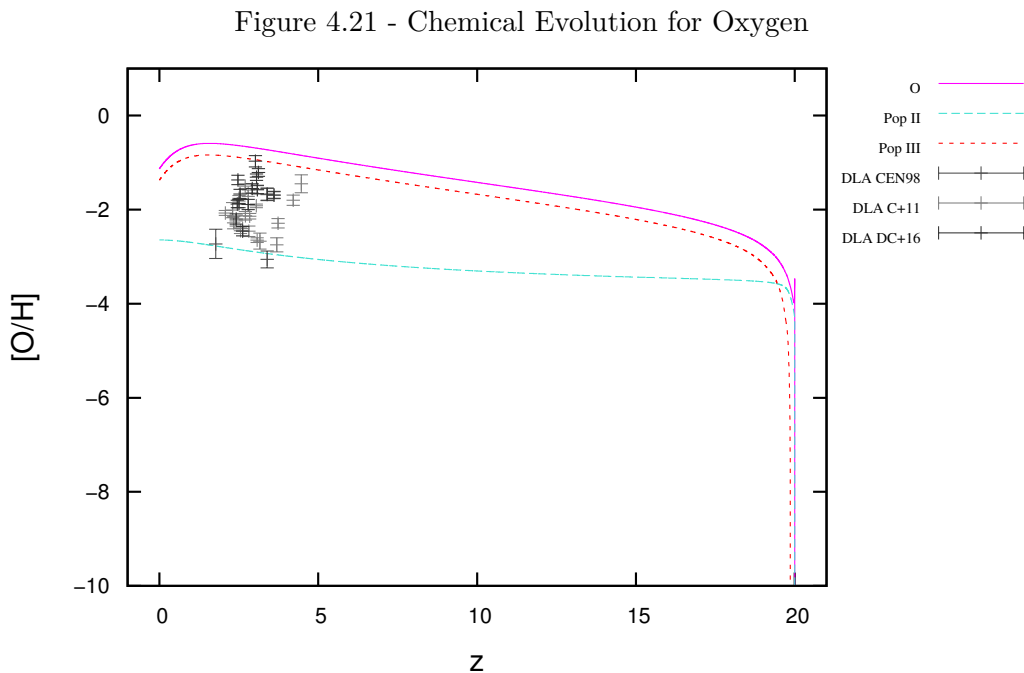


Note: Dust depletion corrected abundances appear to suit better the model. In fact, a quick χ^2 analysis between raw observed values with our model gives $\chi^2_{obs} = 78.93$ while comparison from dust depleted correction of the same data and our model gives $\chi^2_{corr} = 18.19$.

4.3.6 The Carbon, Nitrogen and Oxygen Superabundances

Carbon, Nitrogen and Oxygen nucleosynthesis are dominated by type II SNe - and in the case of Pop III, their production is dominated by PISNe, the typical life-ending for stars with $M > 140M_{\odot}$. PISNe explosions throw a large amount of Oxygen in the IGM, quickly enriching the pristine environment. A $140M_{\odot}$ star, for example, throws $49.2M_{\odot}$ of ^{16}O during the explosion (HEGER; WOOSLEY, 2002). In Figure 4.21, it is possible to see that the final curve for our model (pink curve) is much closer from the Pop III curve, indicating that Pop III nucleosynthesis dominates the production of O in the Universe.

As for Nitrogen and Carbon, Pop III $140M_{\odot}$ star yields $7.9410^{-5}M_{\odot}$ of ^{14}N and $6.89M_{\odot}$ of ^{12}C (HEGER; WOOSLEY, 2002), and in both cases it is Pop II nucleosynthesis that dominates the production of these two metals.



Regarding observations in DLAs, O is only mildly refractory, not being highly affected by depletion, but it is challenging to be observed because the majority of the lines fall into the Ly- α Forest and tend to be saturated. C is also mildly refractory and depletion should not be a great problem for this element (PROCHASKA; WOLFE, 2002).

Figure 4.22 - Chemical Evolution for Nitrogen

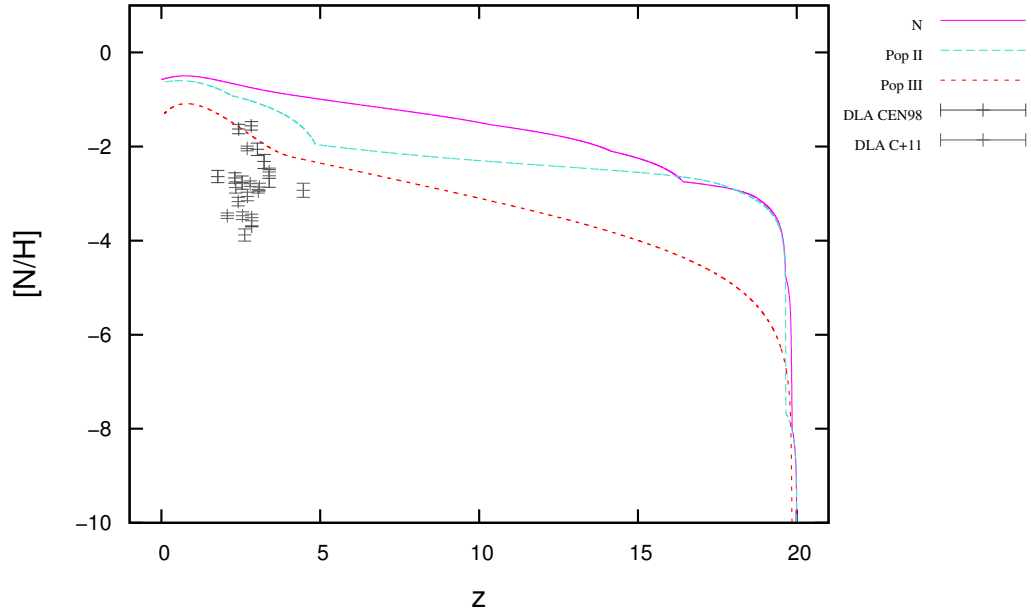
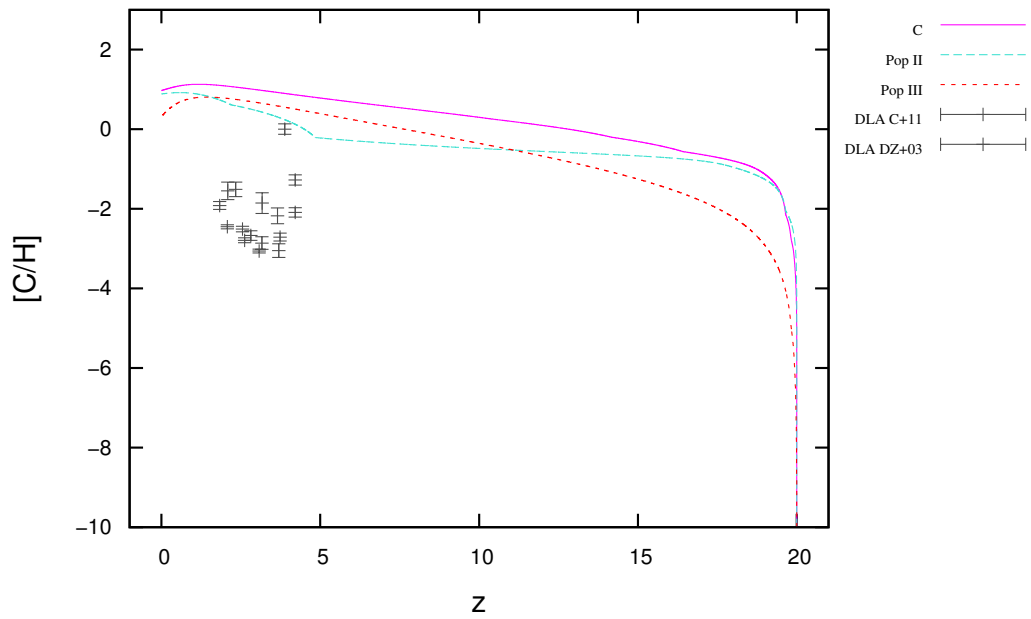


Figure 4.23 - Chemical Evolution for Carbon



Another point to be explored in this matter is the appearance of planets and life in the early Universe. If the model can be best adjusted with the inclusion of SNe Ia and HNe but still shows overabundance of O and C , there should be another mechanism that takes these two elements from the IGM that is not being taken into account. Oxygen and Carbon, along with Nitrogen, Sulfur and Phosphorus are the most important elements for life formation. Carbon and Iron are two elements strongly important for the formation of earth-like planets, and Iron is overabundant in the model too (partially because of depletion as seen before).

Carbon-Enhanced Metal-Poor stars (CEMPs) from the second generation of stars may have planetary systems in their habitable zones, with planets likely made mainly by Carbon (LOEB, 2016). Also, the degree of Carbon enhancement in CEMP stars has been shown to notably increase as a function of decreasing metallicity (LOEB, 2016; CAROLLO et al., 2012), i.e, the Carbon enhancement in these type of stars is likely much higher in the primordial Universe. Another work (SONNENTRUCKER et al., 2010) shows that the abundance of water vapor in gas clouds in the Galaxy uses $\sim 0.1\%$ of the available Oxygen.

If we can build a function for the removal of these elements for the formation of Carbon planets and life along with redshift, it should lead to an interesting discussion about at which level the Chemical Evolution of the Universe is linked with the appearance of planets and life since the formation of the Primordial Stars.

4.3.7 The Sulfur Cosmic Chemical Evolution

Sulfur is the best adjusted element in the model. It is one of the only real non-refractory elements, indicating that it is not affected by depletion (PROCHASKA; WOLFE, 2002).

Figure 4.24 - Chemical Evolution for Sulphur

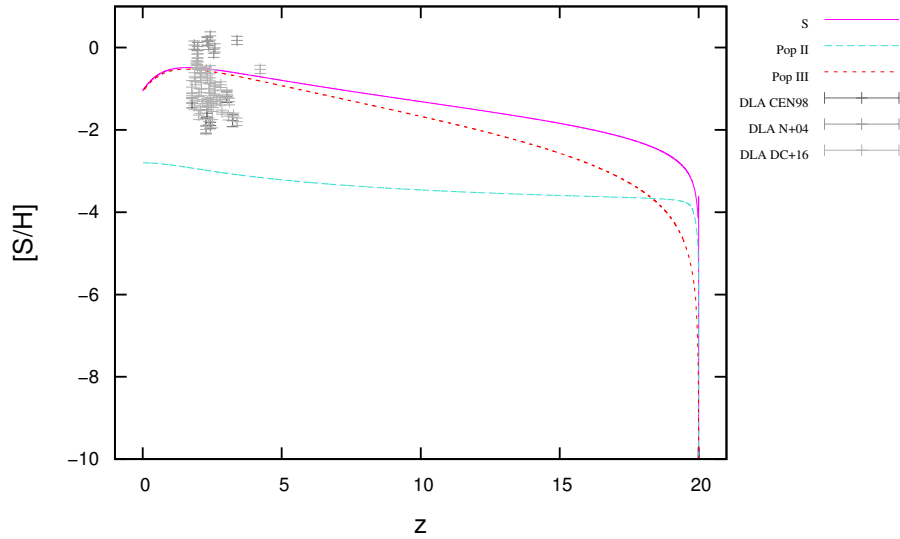
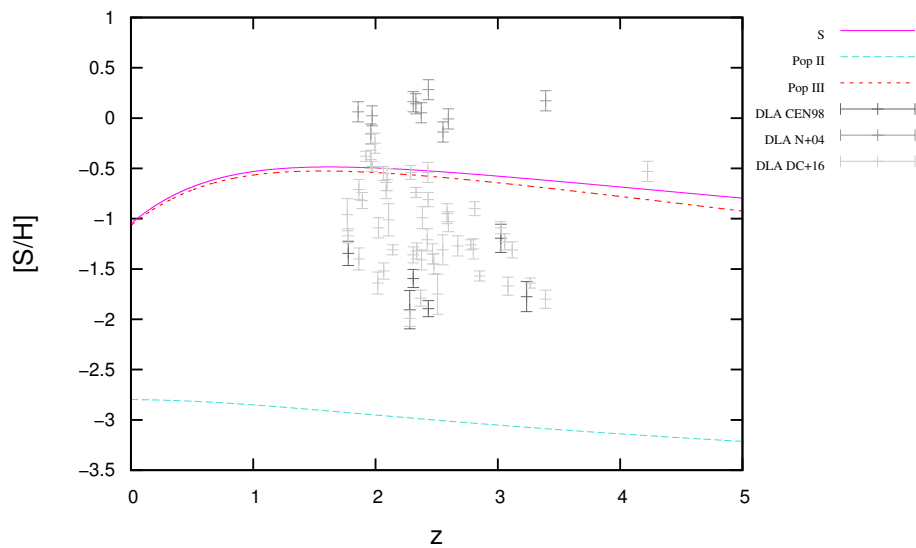


Figure 4.25 - Chemical Evolution for Sulphur - detail



4.3.8 Transition and Z_{cr}

The value for Z_{cr} is discussed to be between 10^{-6} and $10^{-3}Z_{\odot}$ (SCHNEIDER, 2010; MAIO et al., 2010; TORNATORE et al., 2007a; FANG; CEN, 2004; SANTORO; SHULL, 2006). Results from our model indicate that the transition must have occurred very soon (around redshift $z \sim 19$). At $z \sim 20$, the first Pop III stars start to die and inject metals in the IGM, quickly polluting the medium and increasing Total Metallicity. Below we see at which redshift each metallicity is reached. We compare values for Total Metallicity in terms of Solar Metallicity (Fig. 4.26) and also compared to Hydrogen $[Z_{tot}/H]$ (Figs. 4.27 and 4.28). It is expected from the Total Metallicity calculated by the code to be lower than observed values once we know there are several metal production mechanisms that are not being taken into account in the present version of the model.

Table 4.2 - Redshifts at which the model reaches the Metallicities used in the code for the Transition of Populations.

Redshift	Metallicity (Z_{\odot})
19.99667	10^{-6}
19.78833	10^{-4}
18.82333	10^{-3}
16.42333	4.10^{-3}
14.16500	8.10^{-3}
10.35833	2.10^{-2}

Figure 4.26 - Total Metallicity

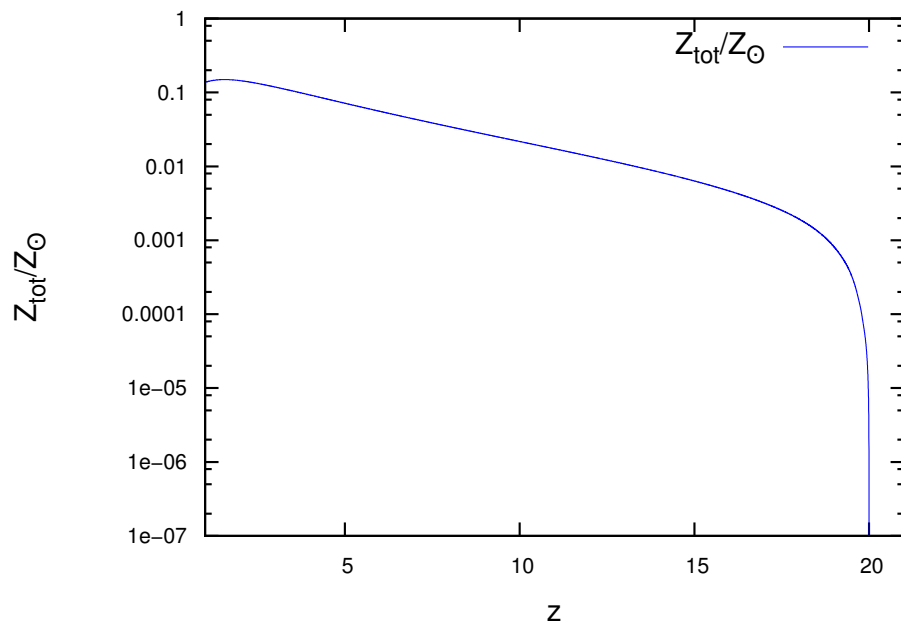


Figure 4.27 - Total Metallicity

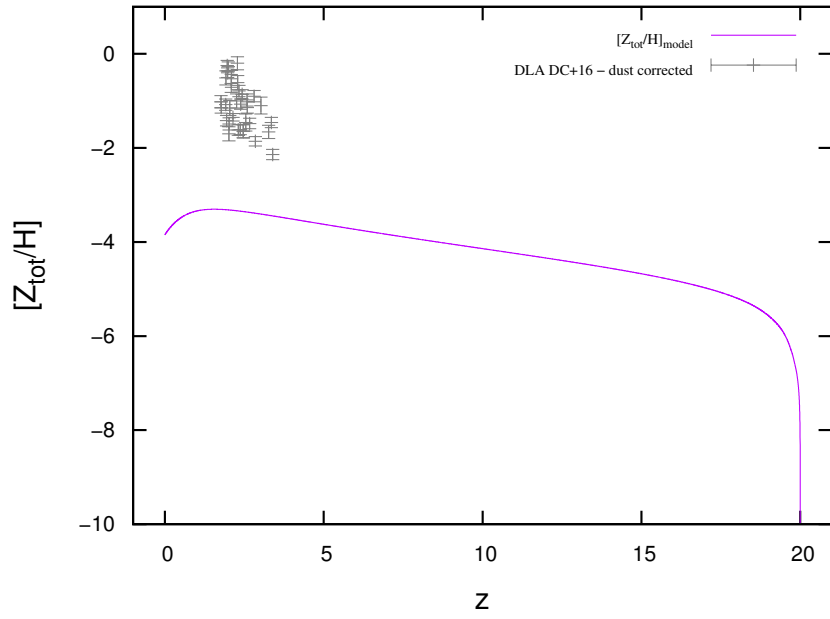
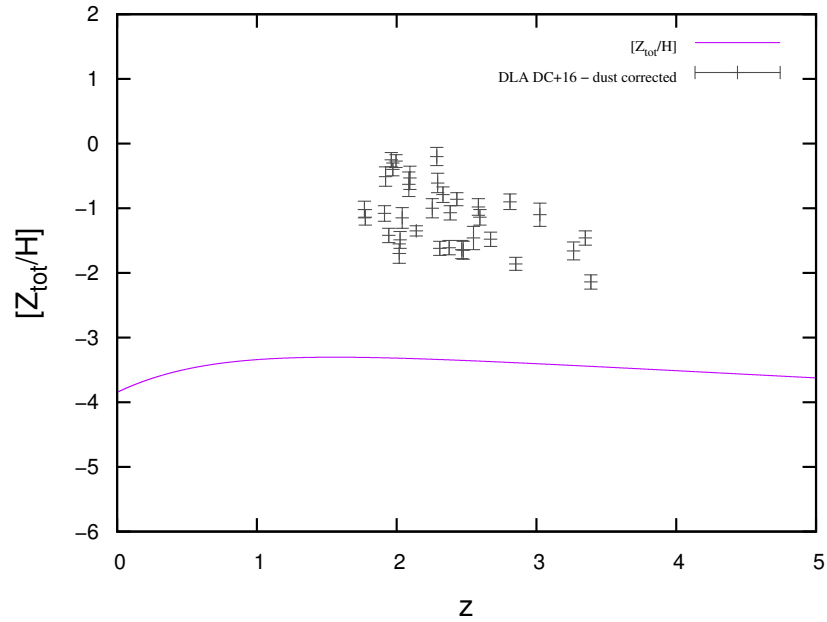


Figure 4.28 - Total Metallicity



5 CONCLUSIONS AND PERSPECTIVES

5.1 Conclusions

The model proposed in this work was developed for studying the evolution of the formation of metals in the Universe since the formation of the First Stars until today, what we call Cosmic Chemical Evolution. By coupling a Cosmological Code with Chemical Evolution Models, we developed a model that calculates the role of Population III and II metal productions along the evolution of the Universe.

With the results, we first concluded that Pop III stars are absolutely essential for reproducing the right level of abundances determined in Damped Lyman- α Systems. It is clear that taking into account only Pop II, the model is completely unable to describe the Chemical Evolution of the Universe. This result gives one more evidence that Pop III-like stars must have existed in the early Universe in order for Chemical Evolution to be explained with accuracy today.

Besides Pop III and Pop II stars, ending their lives as PISNe and regular SNe II, there are other phenomena which could have very important roles in the chemical evolution: Hypernovae and Supernovae type Ia.

Hypernovae use mainly *O*, *C* and *Al* as fuel to produce large amounts of *Si*, *Ca*, *Ti* and *Zn*. With the underabundance of Zinc and superabundance of *O* and *C* in the model, HNe could play an important role in improving those measures. Supernovae type Ia produce a significant amount of heavy elements such as *Cr*, *Ti*, *Fe*, *Ni*, *Mg*, *Si*, *S*, *Ca* and *P*. Consequently, it would help to improve Phosphorus and Nickel underabundances. It even produces more *Ni* than *P*, what it good as the model needs more *Ni* enhancement than *P*.

Another problem is DLA accuracies. DLAs are the best objects to compare with our model because they provide the most accurate chemical abundances in the gas phase. Although they cover a narrow band compared to our redshift range, they are the most distant objects with chemical abundances determined with such precision. However, there are still some problems. Some metal lines blend into the Ly- α Forest making it very hard to determine with precision some abundances. The line for Al II $\lambda 1670$, for example, is strongly saturated and blended with the Ly- α lines for the majority of the systems. As for *Mg*, a careful look on upper limits of DLAs measures revealed a problem in the measures on the work of [Dessauges-Zavadsky et al. \(2002\)](#). For solving this problems, the best strategy is to use only very accurate measures from higher resolution spectra found in the literature.

Another problem from DLAs is depletion. As discussed before, part of the metals are refractory and also get “trapped” into dust grains, reflecting in the spectra

less amount of certain metals than it should show. *Fe* and *Si* are affected by dust and that should be the problem why they look overabundant. Another evidence is that *Fe* is more overabundant than *Si*, which is less affected by depletion than the first. With abundances raising, our model would be able to represent the abundances much better. There is an undetermination of wheater *Al* is affected or not by dust depletion. Another possibility is a higher mass branch of stars with 500 and 1000 M_{\odot} (OHKUBO et al., 2006), which produces large amounts of *Zn*, *P* and *Ni*, compared to *O*, *C* and other metals, and could rise the abundances of these three underabundant metals without raising others too much such as *O* and *C*, which are overabundant. On Table 5.1 it is possible to see a summary of the elements behaviour and possibilities of improvement on the results.

Table 5.1 - Possibilities of abundances problems in the code.

Element	Behaviour in the model	HNe	SNe Ia	Ohkubo	Depletion	DLA measure problems	Another mechanism	
							Formation of planets and life?	Cooling of the gas
Zn	-	✓		✓				
Al	-					✓		
Mg	-				✓	✓		
P	-		✓	✓				
Ni	-		✓	✓				
Fe	+				✓			
Si	+				✓			
C	+	✓					✓	✓
N	+						✓	✓
O	+	✓					✓	✓
S	OK							

Note: symbol - represents underbundance and + overabundance.

As for the Transition, it is needed to develop a higher level version of the code where Pop III and Pop II can coexist, giving the possibility for lower mass Pop III stars to live longer even with the Total Metallicity increasing - that way it will be possible to study the influences of the transition happening at much higher metallicities as discussed, for example, in Smith e Sigurdsson (2007). There is also the possibility of Zero metallicity stars being formed in much lower redshifts ($z \sim 7$) as proposed by (TORNATORE et al., 2007b) what could influence the Total Metallicity in the lower redshift Universe.

A series of mechanisms able to improve the model were discussed and the right combination of them appears to fit well the necessities of improvement for the

code. Once the code is “lacking” some information, it is clear that it is physically consistent and reproduces the abundances according to the informations on which it works on.

5.2 Perspectives

For the first perspectives for the evolution of this work, the yields from the probable other mechanisms lacking in the current version of the code are going to be implemented. SNe Ia rates (MAOZ; MANNUCCI, 2012) and yields (TOWNSLEY et al., 2016) as well as Hypernovae yields (NOMOTO et al., 2006b) and the higher mass branch (500 and $1000M_{\odot}$) yields (OHKUBO et al., 2006) are going to be included. This strategy should raise Zn , P and Ni abundances without raising other elements that are well represented.

Gathering more DLA data with the most reliability possible is also important to improve the comparison with some elements such as Ni , Mg and Al .

Methods for dust depletion correction are also going to be studied in order to apply correction in the data to be compared for affected elements, such as Fe and Si . Also, with the application the depletion correction methods and minor adjustments in the code, it would be also possible to improve depletion correction through the results on the code. It could also help as an extra tool for investigating the reliability of DLA measurements. We intend to understand better the role of dust and its formation during Pop III SNe type II explosions as discussed in the work developed by Marassi et al. (2015).

We intend to develop a version of the code to calculate the gas cooling function of metals. To understand better why C , N and O are overabundant, that could be a good strategy along with studying the formation of CEMP stars, Carbon planets and life inspired by the work developed by Loeb (2016). With the model each step more accurate, the transition between Pop III and Pop II stars could be better understood. To conclude, a citation by Loeb (2016) provides incitement for further investigations on applications of the model developed on this work:

“The questions of when, where, and how the first planetary systems actually formed in cosmic history remain crucial to our understanding of structure formation and the emergence of life in the early Universe. The short-lived, metal-free, massive first-generation stars ultimately exploded as supernovae (SNe) and enriched the interstellar medium (ISM) with the heavy elements fused in their cores. The enrichment of gas with metals that had otherwise been absent in the early Universe enabled the

formation of the first low-mass stars, and perhaps, marked the point at which star systems could begin to form planets. In the core accretion model of planet formation, elements heavier than hydrogen and helium are necessary not only to form the dust grains that are the building blocks of planetary cores, but to extend the lifetime of the protostellar disk long enough to allow the dust grains to grow via merging and accretion to form planetesimals. [...]

The known forms of terrestrial life involve carbon-based chemistry in liquid water. In the cosmological context, life could not have started earlier than 10 Myr after the Big Bang ($z \sim 140$) since the entire Universe was bathed in a thermal radiation background above the boiling temperature of liquid water. Later on, however, the Universe cooled to a habitable epoch at a comfortable temperature of 273 – 373K between 10 – 17 Myr after the Big Bang. [...]

In the past four decades, a broad search has been launched for low-mass Population II stars in the form of extremely metal-poor sources within the halo of the Galaxy. [...] Although these iron-poor stars are often referred to in the literature as 'metal-poor stars', it is critical to note that $[Fe/H]$ does not necessarily reflect a stellar atmosphere's total metal content [...] since many of these stars exhibit large overabundances of elements such as C, N, and O; the total mass fractions, Z , of the elements heavier than He are therefore not much lower than the solar value in these iron-poor stars. Carbon-enhanced metal-poor (CEMP) stars comprise one such chemically anomalous class of stars. [...] Given the significant frequency and level of carbon-excess in this subset of metal-poor Population II stars, the formation of carbon planets around CEMP stars in the early universe presents itself as an intriguing possibility."

REFERENCES

- ADLER, R. J. **The geometry of random fields**. [S.l.]: John Wiley & Sons Inc, 1981. (Wiley Series in Probability and Statistics). ISBN 0471278440,9780471278443. 19
- AKERMAN, C. J.; ELLISON, S. L.; PETTINI, M.; STEIDEL, C. C. Zn and cr abundances in damped lyman alpha systems from the corals survey. **Astronomy & Astrophysics**, v. 440, p. 499–509, set. 2005. 44, 45
- AOKI, W.; SUDA, T.; BEERS, T. C.; HONDA, S. High-resolution spectroscopy of extremely metal-poor stars from sdss/segue. ii. binary fraction. **The Astronomical Journal**, v. 149, p. 39, fev. 2015. 35
- ASPLUND, M.; GREVESSE, N.; SAUVAL, A. J.; SCOTT, P. The chemical composition of the sun. **Annual Review of Astronomy and Astrophysics**, v. 47, n. 1, p. 481–522, 2009. 45, 46
- BALANTEKIN, A. B.; TAKIGAWA, N. Quantum tunneling in nuclear fusion. **Reviews of Modern Physics**, v. 70, p. 77–100, jan. 1998. 26
- BARDEEN, J. M.; BOND, J. R.; KAISER, N.; SZALAY, A. S. The statistics of peaks of gaussian random fields. **The Astrophysical Journal**, v. 304, p. 15–61, maio 1986. 5
- BEVINGTON, D. K. R. P. **Data reduction and error analysis for physical sciences**. 3rd. ed. McGraw-Hill Science/Engineering/Math, 2002. ISBN 9780072472271,0072472278. Disponível em: <<http://gen.lib.rus.ec/book/index.php?md5=8F77E98E9E530D5827FD31322828AF7D>>. 47
- BLOECKER, T. Stellar evolution of low- and intermediate-mass stars. ii. post-agb evolution. **Astronomy & Astrophysics**, v. 299, p. 755, jul. 1995. 43
- BROMM, V.; LOEB, A. The formation of the first low-mass stars from gas with low carbon and oxygen abundances. **Nature**, v. 425, p. 812–814, out. 2003. 34, 35
- CAFFAU, E.; BONIFACIO, P.; SPITE, M.; SPITE, F.; MONACO, L.; SBORDONE, L.; FRANCOIS, P.; GALLAGHER, A. J.; PLEZ, B.; ZAGGIA, S.; LUDWIG, H.-G.; CAYREL, R.; KOCH, A.; STEFFEN, M.; SALVADORI, S.; KLESSEN, R.; GLOVER, S.; CHRISTLIEB, N. Topos: Iii. an ultra iron-poor multiple cemp system. **ArXiv e-prints**, out. 2016. 35

- CAI, Z.; FAN, X.; JIANG, L.; BIAN, F.; MCGREER, I.; DAVÉ, R.; EGAMI, E.; ZABLUDOFF, A.; YANG, Y.; OH, S. P. Probing population iii stars in galaxy iok-1 at $z = 6.96$ through he ii emission. **The Astrophysical Journal**, v. 736, p. L28, ago. 2011. 35
- CAI, Z.; FAN, X.; JIANG, L.; DAVÉ, R.; OH, S. P.; YANG, Y.; ZABLUDOFF, A. Constraining very high mass population iii stars through he ii emission in galaxy bdf-521 at $z = 7.01$. **The Astrophysical Journal**, v. 799, p. L19, fev. 2015. 35
- CAMPBELL, S. W.; LATTANZIO, J. C. Evolution and nucleosynthesis of extremely metal-poor and metal-free low- and intermediate-mass stars. i. stellar yield tables and the cemps. **Astronomy & Astrophysics**, v. 490, p. 769–776, nov. 2008. 35, 41, 48
- CAROLLO, D.; BEERS, T. C.; BOVY, J.; SIVARANI, T.; NORRIS, J. E.; FREEMAN, K. C.; AOKI, W.; KENNEDY, Y. S. L. C. R. Carbon-enhanced metal-poor stars in the inner and outer halo components of the milky way. **The Astrophysical Journal**, v. 744, n. 2, p. 195, 2012. 65
- CARROLL, B.; OSTLIE, D. **An introduction to modern astrophysics**. 2ed., pearson. ed. [S.l.: s.n.], 2007. ISBN 0321442849,9780321442840. 37
- CENTURIÓN, M.; BONIFACIO, P.; MOLARO, P.; VLADILO, G. Nitrogen abundances in damped $\text{ly}\alpha$ galaxies. **The Astrophysical Journal**, v. 509, p. 620–632, dez. 1998. 44
- Cescutti, G.; Matteucci, F.; Caffau, E.; François, P. Chemical evolution of the milky way: the origin of phosphorus. **Astronomy & Astrophysics**, v. 540, p. A33, abr. 2012. 56
- CHIEFFI, A.; LIMONGI, M. Explosive yields of massive stars from $z = 0$ to $z = z_{\odot}$. **The Astrophysical Journal**, v. 608, n. 1, p. 405, 2004. 43
- CIA, A. D.; LEDOUX, C.; MATTSSON, L.; PETITJEAN, P.; SRIANAND, R.; GAVIGNAUD, I.; JENKINS, E. B. Dust-depletion sequences in damped lyman- α absorbers. a unified picture from low-metallicity systems to the galaxy. **Astronomy & Astrophysics**, v. 596, p. A97, dez. 2016. 45, 54
- CIA, A. D.; LEDOUX, C.; SAVAGLIO, S.; SCHADY, P.; VREESWIJK, P. M. Dust-to-metal ratios in damped lyman- α absorbers. fresh clues to the origins of dust and optical extinction towards γ -ray bursts. **Astronomy & Astrophysics**, v. 560, p. A88, dez. 2013. 59

COOKE, R.; PETTINI, M.; JORGENSEN, R. A.; MURPHY, M. T.; RUDIE, G. C.; STEIDEL, C. C. The explosion energy of early stellar populations: the fe-peak element ratios in low-metallicity damped $\text{ly}\alpha$ systems. **Monthly Notices of the Royal Astronomical Society**, v. 431, p. 1625–1637, maio 2013. [47](#)

COOKE, R.; PETTINI, M.; STEIDEL, C. C.; RUDIE, G. C.; NISSEN, P. E. The most metal-poor damped $\text{ly}\alpha$ systems: insights into chemical evolution in the very metal-poor regime. **Monthly Notices of the Royal Astronomical Society**, v. 417, p. 1534–1558, out. 2011. [44](#)

COPI, C. J. A stochastic approach to chemical evolution. **The Astrophysical Journal**, v. 487, n. 2, p. 704, 1997. [31](#)

DAIGNE, F.; OLIVE, K. A.; SILK, J.; STOEHR, F.; VANGIONI, E. Hierarchical growth and cosmic star formation: Enrichment, outflows, and supernova rates. **The Astrophysical Journal**, v. 647, p. 773–786, ago. 2006. [20](#)

DESSAUGES-ZAVADSKY, M.; PÉROUX, C.; KIM, T.-S.; D'ODORICO, S.; MCMAHON, R. G. A homogeneous sample of sub-damped lyman α systems - i. construction of the sample and chemical abundance measurements. **Monthly Notices of the Royal Astronomical Society**, v. 345, p. 447–479, out. 2003. [44](#), [52](#), [54](#)

DESSAUGES-ZAVADSKY, M.; PROCHASKA, J. X.; D'ODORICO, S. New detections of mn, ti and mg in damped lyalpha systems: Toward reconciling the dust/nucleosynthesis degeneracy. **Astronomy & Astrophysics**, v. 391, p. 801–807, set. 2002. [44](#), [54](#), [55](#), [71](#)

DODELSON, S. **Modern cosmology**. 1. ed. [S.l.]: Academic Press, 2003. ISBN 0122191412,9780122191411,9780080511979. [5](#)

DOHERTY, C. L.; GIL-PONS, P.; LAU, H. H. B.; LATTANZIO, J. C.; SIESS, L. Super and massive agb stars - ii. nucleosynthesis and yields - $z = 0.02, 0.008$ and 0.004 . **Monthly Notices of the Royal Astronomical Society**, v. 437, p. 195–214, jan. 2014. [43](#)

DOHERTY, C. L.; GIL-PONS, P.; LAU, H. H. B.; LATTANZIO, J. C.; SIESS, L.; CAMPBELL, S. W. Super and massive agb stars - iii. nucleosynthesis in metal-poor and very metal-poor stars - $z = 0.001$ and 0.0001 . **Monthly Notices of the Royal Astronomical Society**, v. 441, p. 582–598, jun. 2014. [43](#)

ELLISON, S. L.; KANEKAR, N.; PROCHASKA, J. X.; MOMJIAN, E.;
WORSECK, G. H. i content, metallicities and spin temperatures of damped and
sub-damped $\text{Ly}\alpha$ systems in the redshift desert ($0.6 < z_{\text{abs}} < 1.7$)^a. **Monthly Notices
of the Royal Astronomical Society**, v. 424, p. 293–312, jul. 2012. xi, 39

FANG, T.; CEN, R. The transition from population iii to population ii stars. **The
Astrophysical Journal**, v. 616, p. L87–L90, dez. 2004. 36, 67

FREBEL, A.; NORRIS, J. E. Near-field cosmology with extremely metal-poor
stars. **Annual Review of Astronomy and Astrophysics**, v. 53, p. 631–688,
ago. 2015. 35

FROST, C.; LATTANZIO, J. C. On the numerical treatment and dependence of
the third dredge-up phenomenon. **The Astrophysical Journal**, v. 473, n. 1992, p.
383–387, 1996. ISSN 15384357. 43

HEGER, A.; WOOSLEY, S. E. The nucleosynthetic signature of population iii.
The Astrophysical Journal, IOP Publishing, v. 567, n. 1, p. 532, 2002. xi, 32,
34, 35, 41, 48, 63

_____. Nucleosynthesis and evolution of massive metal-free stars. **The
Astrophysical Journal**, v. 724, n. 1, p. 341, 2010. 34, 41, 48

HOU, J. L.; BOISSIER, S.; PRANTZOS, N. Chemical evolution and depletion
pattern in damped lyman alpha systems. **Astronomy & Astrophysics**, v. 370,
p. 23–33, abr. 2001. 37

IGLESIAS, C. A.; ROGERS, F. J. Updated opal opacities. **The Astrophysical
Journal**, v. 464, p. 943, jun. 1996. 43

KARAKAS, A. I. Updated stellar yields from asymptotic giant branch models.
Monthly Notices of the Royal Astronomical Society, Blackwell Publishing
Ltd, v. 403, n. 3, p. 1413–1425, 2010. ISSN 1365-2966. 43

KIPPENHAHN, A. W. R. **Stellar Structure and Evolution [Study edn]**.
[S.l.]: Springer, 1989. 26

KULKARNI, V. P.; MEIRING, J.; SOM, D.; PEROUX, C.; YORK, D. G.;
KHARE, P.; LAUROESCH, J. T. A super-damped lyman-alpha qso absorber at
 $z=2.2$. **ArXiv e-prints**, fev. 2012. 45

- LARSON, R. B.; TINSLEY, B. M.; CALDWELL, C. N. The evolution of disk galaxies and the origin of s0 galaxies. **The Astrophysical Journal**, v. 237, p. 692–707, maio 1980. [33](#)
- LOEB, A. On the habitability of our universe. **ArXiv e-prints**, jun. 2016. [vii](#), [ix](#), [65](#), [73](#)
- MACIA, E. The role of phosphorus in chemical evolution. **Chemical Society Reviews**, The Royal Society of Chemistry, v. 34, p. 91–701, 2005. [56](#)
- MAIO, U.; CIARDI, B.; DOLAG, K.; TORNATORE, L.; Khochfar, S. The transition from population iii to population ii-i star formation. **Monthly Notices of the Royal Astronomical Society**, v. 407, p. 1003–1015, set. 2010. [36](#), [67](#)
- MAIO, U.; TESCARI, E. Origin of cosmic chemical abundances. **Monthly Notices of the Royal Astronomical Society**, v. 453, p. 3798–3820, nov. 2015. [44](#)
- MAOZ, D.; MANNUCCI, F. Type-ia supernova rates and the progenitor problem: A review. **Publications of the Astronomical Society of Australia**, v. 29, p. 447–465, jan. 2012. [73](#)
- Marassi, S.; Schneider, R.; Limongi, M.; Chieffi, A.; Bocchio, M.; Bianchi, S. The metal and dust yields of the first massive stars. **Monthly Notices of the Royal Astronomical Society**, v. 454, p. 4250–4266, dez. 2015. [73](#)
- MATTEUCCI, F. **The chemical evolution of the Galaxy**. [S.l.: s.n.], 2001. [26](#)
- _____. Introduction to galactic chemical evolution. **Journal of Physics Conference Series**, v. 703, n. 1, p. 012004, abr. 2016. [1](#)
- _____. _____. **ArXiv e-prints**, 2016. [32](#)
- NISSEN, P. E.; CHEN, Y. Q.; ASPLUND, M.; PETTINI, M. Sulphur and zinc abundances in galactic stars and damped $\text{Ly}\alpha$ systems. **Astronomy & Astrophysics**, v. 415, p. 993–1007, mar. 2004. [45](#)
- NOMOTO, K.; IWAMOTO, K.; NAKASATO, N.; THIELEMANN, F.-K.; BRACHWITZ, F.; TSUJIMOTO, T.; KUBO, Y.; KISHIMOTO, N. Nucleosynthesis in type ia supernovae. **Nuclear Physics A**, v. 621, n. 1, p. 467 – 476, 1997. ISSN 0375-9474. [56](#)

NOMOTO, K.; KOBAYASHI, C.; TOMINAGA, N. Nucleosynthesis in stars and the chemical enrichment of galaxies. **Annual Review of Astronomy and Astrophysics**, v. 51, p. 457–509, ago. 2013. 39

NOMOTO, K.; TOMINAGA, N.; UMEDA, H.; KOBAYASHI, C.; MAEDA, K. Nucleosynthesis yields of core-collapse supernovae and hypernovae, and galactic chemical evolution. **Nuclear Physics A**, v. 777, p. 424–458, out. 2006. 49

NOMOTO, K.; TOMINAGA, N.; UMEDA, H.; KOBAYASHI, C.; MAEDA, K. Nucleosynthesis yields of core-collapse supernovae and hypernovae, and galactic chemical evolution. **Nuclear Physics A**, v. 777, p. 424–458, out. 2006. 73

OEMLER, A. The cluster of galaxies abell 2670. , v. 180, abr. 1973. 17

OHKUBO, T.; UMEDA, H.; MAEDA, K.; NOMOTO, K.; SUZUKI, T.; TSURUTA, S.; REES, M. J. Core-collapse very massive stars: Evolution, explosion, and nucleosynthesis of population iii 500-1000 mâ stars. **The Astrophysical Journal**, v. 645, n. 2, p. 1352, 2006. xi, 34, 50, 51, 56, 72, 73

O'SHEA, B. W.; MCKEE, C. F.; HEGER, A.; ABEL, T. First stars iii conference summary. In: O'Shea, B. W.; Heger, A. (Ed.). **First Stars III**. [S.l.: s.n.], 2008. (American Institute of Physics Conference Series, v. 990), p. xiii. 35

PADMANABHAN, T. **Structure formation in the Universe**. 1. ed. [S.l.]: Cambridge University Press, 1993. ISBN 0521424860,9780521424868. 5

PEEBLES, P. J. E. **Principles of Physical Cosmology**. [S.l.]: Princeton University Press, 1993. (Princeton series in physics). ISBN 0691074283,9780691074283,0691074283-:,0691019339. 5

PEREIRA, E. S.; MIRANDA, O. D. Stochastic background of gravitational waves generated by pre-galactic black holes. **Monthly Notices of the Royal Astronomical Society**, v. 401, p. 1924–1932, jan. 2010. vii, ix, 2, 21, 23, 33

PETTINI, M.; KING, D. L.; SMITH, L. J.; HUNSTEAD, R. W. Dust in high-redshift galaxies. **The Astrophysical Journal**, v. 478, p. 536–541, mar. 1997. 44

PETTINI, M.; ZYCH, B. J.; STEIDEL, C. C.; CHAFFEE, F. H. C, n, o abundances in the most metal-poor damped lyman alpha systems. **Monthly Notices of the Royal Astronomical Society**, v. 385, p. 2011–2024, abr. 2008. 44, 45

PRESS, W. H.; SCHECHTER, P. Formation of galaxies and clusters of galaxies by self-similar gravitational condensation. **The Astrophysical Journal**, v. 187, p. 425–438, fev. 1974. [12](#), [17](#)

PRIALNIK, D. **An introduction to the theory of stellar structure and evolution**. [S.l.]: Cambridge University Press, 2000. ISBN 052165937X,9780521659376,0521650658. [26](#)

PROCHASKA, J. X.; WOLFE, A. M. The ucsd hires/keck i damped $\text{Ly}\alpha$ abundance database. ii. the implications. **The Astrophysical Journal**, v. 566, p. 68–92, fev. 2002. [52](#), [59](#), [63](#), [66](#)

Prochaska, J. X.; Wolfe, A. M.; Howk, J. C.; Gawiser, E.; Burles, S. M.; Cooke, J. The UCSD/Keck Damped $\text{Ly}\alpha$ Abundance Database: A Decade of High-Resolution Spectroscopy. **The Astrophysical Journal**, v. 171, p. 29–60, jul. 2007. [44](#), [45](#)

RAUCH, M. Lyman alpha forest. In: _____. **Encyclopedia of Astronomy and Astrophysics**. [S.l.: s.n.], 2000. [37](#)

RAUSCHER, T.; PATKÓŠ, A. Handbook of nuclear chemistry. In: _____. [S.l.]: Springer US, 2011. cap. Origin of the Chemical Elements, p. 611–665. ISBN 978-1-4419-0720-2. [27](#)

REIMERS, D. Circumstellar absorption lines and mass loss from red giants. **Memoires of the Societe Royale des Sciences de Liege**, v. 8, p. 369–382, 1975. [43](#)

SALPETER, E. E. The rate of star formation in the galaxy. **The Astrophysical Journal**, IOP Publishing, v. 129, n. 1, p. 608, 1959. [21](#)

SANTORO, F.; SHULL, J. M. Critical metallicity and fine-structure emission of primordial gas enriched by the first stars. **The Astrophysical Journal**, v. 643, n. 1, p. 26, 2006. [34](#), [36](#), [67](#)

SCHNEIDER, R. The population iii/ii transition. **AIP Conference Proceedings**, v. 1294, n. 1, 2010. [36](#), [67](#)

SMITH, B. D. **The Transition from Population III to Population II Star Formation in the Early Universe**. Tese (Doutorado) — The Pennsylvania State University, dez. 2007. [34](#), [36](#)

SMITH, B. D.; SIGURDSSON, S. The transition from the first stars to the second stars in the early universe. **The Astrophysical Journal**, v. 661, p. L5–L8, maio 2007. 72

SOBRAL, D.; MATTHEE, J.; DARVISH, B.; SCHAERER, D.; MOBASHER, B.; RÖTTGERING, H. J. A.; SANTOS, S.; HEMMATI, S. Evidence for popiii-like stellar populations in the most luminous lyman- α emitters at the epoch of reionization: Spectroscopic confirmation. **The Astrophysical Journal**, v. 808, p. 139, ago. 2015. 35

SONNENTRUCKER, P.; NEUFELD, D. A.; PHILLIPS, T. G.; GERIN, M.; LIS, D. C.; LUCA, M. de; GOICOECHEA, J. R.; BLACK, J. H.; BELL, T. A.; BOULANGER, F.; CERNICHAO, J.; COUTENS, A.; DARTOIS, E.; KAŹMIERCZAK, M.; ENCRENAZ, P.; FALGARONE, E.; GEBALLE, T. R.; GIESEN, T.; GODARD, B.; GOLDSMITH, P. F.; GRY, C.; GUPTA, H.; HENNEBELLE, P.; HERBST, E.; HILY-BLANT, P.; JOBLIN, C.; KOŁOS, R.; KREŁOWSKI, J.; MARTÍN-PINTADO, J.; MENTEN, K. M.; MONJE, R.; MOOKERJEA, B.; PEARSON, J.; PERAULT, M.; PERSSON, C. M.; PLUME, R.; SALEZ, M.; SCHLEMMER, S.; SCHMIDT, M.; STUTZKI, J.; TEYSSIER, D.; VASTEL, C.; YU, S.; CAUX, E.; GÜSTEN, R.; HATCH, W. A.; KLEIN, T.; MEHDI, I.; MORRIS, P.; WARD, J. S. Detection of hydrogen fluoride absorption in diffuse molecular clouds with herchel/hifi: an ubiquitous tracer of molecular gas. **Astronomy & Astrophysics**, v. 521, p. L12, out. 2010. 65

SPRINGEL, V.; WHITE, S. D. M.; JENKINS, A.; FRENK, C. S.; YOSHIDA, N.; GAO, L.; NAVARRO, J.; THACKER, R.; CROTON, D.; HELLY, J.; PEACOCK, J. A.; COLE, S.; THOMAS, P.; COUCHMAN, H.; EVRARD, A.; COLBERG, J.; PEARCE, F. Simulations of the formation, evolution and clustering of galaxies and quasars. **Nature**, v. 435, p. 629–636, jun. 2005. xi, 3, 5

TINSLEY, B. M.; LARSON, R. B. Chemical evolution and the formation of galactic disks. **The Astrophysical Journal**, v. 221, p. 554–561, abr. 1978. 1, 33

TORNATORE, L.; FERRARA, A.; SCHNEIDER, R. Population iii stars: hidden or disappeared? **Monthly Notices of the Royal Astronomical Society**, v. 382, p. 945–950, dez. 2007. 36, 67

_____. _____. **Monthly Notices of the Royal Astronomical Society**, v. 382, p. 945–950, dez. 2007. 72

TOWNSLEY, D. M.; MILES, B. J.; TIMMES, F. X.; CALDER, A. C.; BROWN, E. F. A tracer method for computing type ia supernova yields: Burning model calibration, reconstruction of thickened flames, and verification for planar detonations. **The Astrophysical Journals**, v. 225, p. 3, jul. 2016. 73

VASSILIADIS, E.; WOOD, P. R. Evolution of low- and intermediate-mass stars to the end of the asymptotic giant branch with mass loss. **The Astrophysical Journal**, v. 413, p. 641–657, ago. 1993. 43

VITTI, M. **Uma contribuição ao estudo do enriquecimento químico do universo**. Dissertação (Mestrado) — Instituto Nacional de Pesquisas Espaciais, São José dos Campos, SP, Brasil, 2012. vii, ix, 39, 40, 45, 49

VLADILLO, G. Dust and elemental abundances in damped $\text{ly}\alpha$ absorbers. **The Astrophysical Journal**, v. 493, p. 583–594, jan. 1998. 45

_____. Chemical abundances of damped $\text{ly}\alpha$ systems: a new method for estimating dust depletion effects. **Astronomy & Astrophysics**, v. 391, p. 407–415, ago. 2002. 38, 39, 45, 59

WOLFE, A. M.; GAWISER, E.; PROCHASKA, J. X. Damped $\text{ly}\alpha$ systems. **Annual Review of Astronomy and Astrophysics**, v. 43, n. 1, p. 861–918, 2005. 37, 38

WOLFIRE, M. G.; MCKEE, C. F.; HOLLENBACH, D.; TIELENS, A. G. G. M. Neutral atomic phases of the interstellar medium in the galaxy. **The Astrophysical Journal**, v. 587, p. 278–311, abr. 2003. 37

PUBLICAÇÕES TÉCNICO-CIENTÍFICAS EDITADAS PELO INPE

Teses e Dissertações (TDI)

Teses e Dissertações apresentadas nos Cursos de Pós-Graduação do INPE.

Manuais Técnicos (MAN)

São publicações de caráter técnico que incluem normas, procedimentos, instruções e orientações.

Notas Técnico-Científicas (NTC)

Incluem resultados preliminares de pesquisa, descrição de equipamentos, descrição e ou documentação de programas de computador, descrição de sistemas e experimentos, apresentação de testes, dados, atlas, e documentação de projetos de engenharia.

Relatórios de Pesquisa (RPQ)

Reportam resultados ou progressos de pesquisas tanto de natureza técnica quanto científica, cujo nível seja compatível com o de uma publicação em periódico nacional ou internacional.

Propostas e Relatórios de Projetos (PRP)

São propostas de projetos técnico-científicos e relatórios de acompanhamento de projetos, atividades e convênios.

Publicações Didáticas (PUD)

Incluem apostilas, notas de aula e manuais didáticos.

Publicações Seriadas

São os seriados técnico-científicos: boletins, periódicos, anuários e anais de eventos (simpósios e congressos). Constam destas publicações o Internacional Standard Serial Number (ISSN), que é um código único e definitivo para identificação de títulos de seriados.

Programas de Computador (PDC)

São a seqüência de instruções ou códigos, expressos em uma linguagem de programação compilada ou interpretada, a ser executada por um computador para alcançar um determinado objetivo. Aceitam-se tanto programas fonte quanto os executáveis.

Pré-publicações (PRE)

Todos os artigos publicados em periódicos, anais e como capítulos de livros.